Journal of Arid Environments (2002) **51**: 281–318
doi:10.1006/jare.2001.0867, available online at http://www.idealibrary.com on IDEAL®

Micrometeorological modeling to understand the thermal anomaly in the sand dunes across the Israel–Egypt border

Zhihao Qin*, Pedro Berliner† & Arnon Karnieli*‡

**The Remote Sensing Laboratory, Department of Environmental Physics, J. Blaustein Institute for Desert Research, Ben Gurion University of the Negev, Sede Boker Campus, 84990, Israel*
†The Wyler Laboratory for Arid Land Conservation and Development, Department of Dryland Agriculture, J. Blaustein Institute for Desert Research, Ben Gurion University of the Negev, Sede Boker Campus, 84990, Israel

(Received 12 April 2000, accepted 23 May 2001)

A thermal anomaly was observed on the remote sensing images in the sand dunes across the Israel–Egypt border. The Israeli side with more vegetation cover has higher ($>2^{\circ}$C) land surface temperature (LST) during the day than the Egyptian side where bare sand prevails. This anomaly is very obvious at about noon in the hot dry summer season. A micrometeorological model has been established in terms of surface energy balance for simulating the surface temperature change and heat flux variation of the region. The purpose of this modeling is to understand the mechanism leading to the occurrence of the thermal anomaly and to reveal the key factors controlling the surface temperature change. The characteristic of the model lies in its coupling soil temperature changing simultaneously with soil moisture movement, described as two differential equations. The methodology for the numerical solution of the model has been developed. The required meteorological data and soil parameters were measured at the study region in the hot summer season for the simulation. Two typical and the most important surface patterns of the region are considered: biogenic crust representing the Israeli side and the bare sand representing the Egyptian side. Results from simulation indicate that surface albedo contributes most to the surface temperature difference between the two typical surfaces, which is followed by sub-soil properties (mainly soil moisture) difference. Biogenic crust has lower surface albedo than bare sand. Consequently, it absorbs much more incident sky radiation. During the hot summer season, the region is very dry and vegetation is in dormancy. The canopy of most shrubs reduces to minimum. Even though the Israeli side has more vegetation, the evapo-transpiration contributed by the vegetation is still very small ($<7\%$) in comparison with the net radiation. This small latent heat flux has little effect on the surface energy balance process in the arid environment. LST change in the desert region is mainly controlled by the amount of incident solar energy absorbed by the ground as soil heat. Therefore, the anomalous LST change and

‡Correspondence to: E-mail: karnieli@bgumail.bgu.ac.il

0140-1963/02/020281 + 38 $35.00/0

thermal variation on both sides of the region can still be explained as the direct result of the obvious albedo difference on both sides. This albedo difference is mainly caused by the sharp contrast of surface composition especially different biogenic crust and bare sand cover rates on both sides. The overgrazing and other anthropogenic stresses are the direct reasons leading to the bare sand (high albedo) prevalent on the Egyptian side while the conservation policy helps the development of biogenic crust and vegetation (low albedo) on the Israeli side.

Keywords: micrometeorological modeling; thermal anomaly; biogenic crust; the Israel—Egypt border

Introduction

The northern part of the Israel–Egypt political border is crossed by linear sand dunes of the same lithological unit, which was formed by the deposition of sand and dust transported from North African desert by strong wind. The sand dune region covers an area of about $30 \times 80\,km^2$ (30 km along the border and a length of about 40 km on both sides). The geomorphological patterns of the region are mainly the linear sand dunes and interdune valleys stretching from the Egyptian side into the Israeli side. Fine sand with a diameter of about 0·01–0·05 mm (Gerson *et al.*, 1985) is the principal material of soil constituents in the region though silt and clay also account for some percentages ($<5\%$) especially on the Israeli side, where a thin biogenic crust covers most of its surface (Karnieli, 1997; Qin, 1998; Qin & Karnieli, 2000). The average annual rainfall of the region is 95 mm (Kidron & Yair, 1997). Rainy season concentrates on the period from November to March of the next year. The altitude of the region is about 74 m above sea level and the distance from the Mediterranean Sea is about 20–50 km (Kidron, 1999).

In remote sensing images of visible channels such as Fig. 1, this region is characterized by a sharp contrast between the bright reflectance from the Egyptian

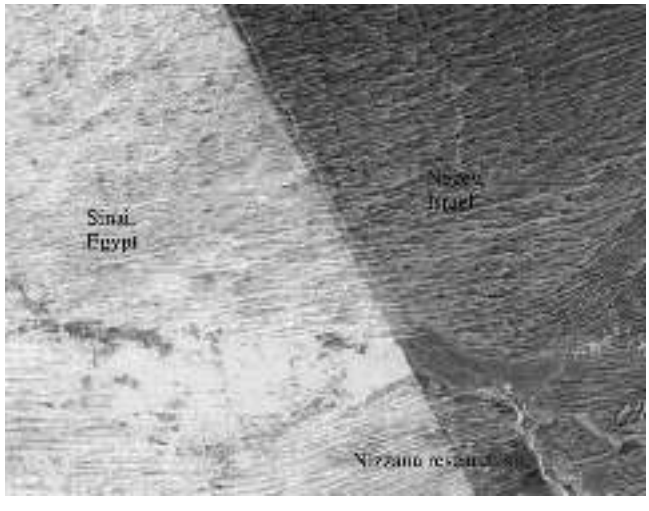

Figure 1. Spectral contrast on both sides of the Israel–Egypt border, false color composition of Landsat TM 4, 3 and 2, acquired on March 29, 1995.

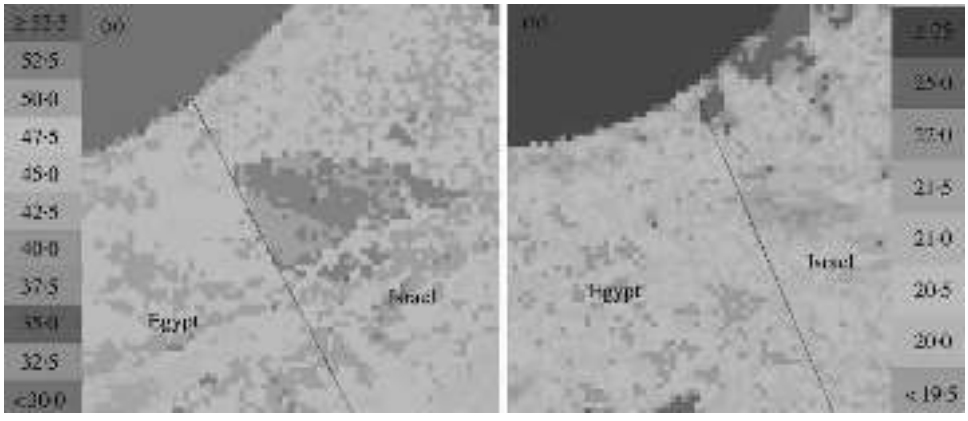

Figure 2. Thermal variation of the region, retrieved from NOAA-AVHRR data acquired on July 18, 1998. An obvious LST difference can be seen on both sides of the border in the daytime image (a) and this difference disappears in the night-time image (b).

side (Sinai) and the dark one from the Israeli side (Negev) (Tsoar & Karnieli, 1996). The contrast was interpreted as being caused by different land surface cover structures under different land use policies (Otterman, 1974, 1977, 1981; Warren & Harrison, 1984; Tsoar & Møller, 1986). The Egyptian side has lower vegetation cover and much more bare sand surface. In contrast, the Israeli side is dominated by much more shrubs and inactive sand surface fixed by biogenic crust, which contains several active microphytes especially cyanobacteria (Karnieli *et al.*, 1996; Karnieli & Sarafis, 1996). Thus, the crust was also named as microbial crust (Kidron & Yair, 1997). The thin biogenic crust (<5 mm) mainly concentrates on the lower part of the longitudinal dunes in the western Negev, Israel and is very few on the Egyptian side due to its intensive anthropogenic activities (Tsoar & Møller, 1986).

Karnieli & Tsoar (1995) suggested a different interpretation of the spectral contrast. In summary, three types of evidence have been combined to verify the hypothesis explaining the difference in spectral reflectance on the opposite sides of the border. (1) Vegetation cover in the region is less than 20% and therefore soil is believed to be the principal contributor to the overall spectral reflectance of the region. (2) The spectral reflectance of the arid dune vegetation is much lower than that of the bare sand and biogenic crust. Consequently, the dune vegetation signal is masked by soil signal in terms of remote sensing. (3) The biogenic crust covering most of the Israeli side contributes a darker tone to remote sensing images. Anthropogenic activities on the Egyptian side that prevent the establishment of the crust contribute to the brighter tone. Therefore, it is concluded that the well-known contrast between Sinai and Negev in remote sensing imagery that has drawn the attention of many scientists is not a direct result of vegetation cover but caused by almost complete cover of biogenic crust (Karnieli & Tsoar, 1995).

The sharp spectral contrast between the two sides of the Israel–Egypt border is not only observed in visible channels but also in thermal ones. On the daytime thermal images of remote sensing, the Israeli side is observed to have higher land surface temperature (LST) than the Egyptian side (Fig. 2(a)). This phenomenon occurs not on a specific day but almost throughout the year except the days when the ground is very wet and cool. Remote sensing analysis of the NOAA–AVHRR data for 1995–1998 (Qin *et al.*, 2000) indicates that in the dry summer season in the early afternoon (13:00–15:00) when the data were acquired, the Israeli side is generally about 2–3.5°C hotter than the Egyptian side. In the wet winter season, LST on the Israeli

side is also higher than on the Egyptian side. Usually, the Israeli side has an average LST of 0·5–1·5°C higher than the Egyptian side in the wet winter season. Only in a few extreme cases when the surface was very wet after heavy rain did the Egyptian side have a little bit higher LST than the Israeli side. However, the LST difference in these extreme cases is generally within −0·5°C (Qin *et al.*, 2000). Considering more vegetation cover on the Israeli side, this phenomenon of temperature difference in the border region is really anomalous. The sharp LST contrast on both sides disappears in the night-time images (Fig. 2(b)), when the LST change of the region at about midnight is mainly within the range of 18–23°C during the summer season.

Otterman (1974) firstly reported this thermal contrast. Using an infrared thermometer mounted on an airplane flying in the region, he discovered that the maximum temperature difference across the demarcation line was up to 5°C at about 14:00 in July. He related the contrast to severe overgrazing and other anthropogenic pressures on the Egyptian side. After analysing the impact of these pressures, he concluded that in an arid climate, under the semi-dormant conditions of vegetation, which prevail at all times except for the short desert blooming period after rains, evapo-transpiration is very low and has apparently a negligible effect on the surface temperature. Thus, LST of desert region is controlled by the surface albedo (Otterman, 1974). The importance of albedo in affecting the climatic features especially precipitation, air temperature, etc. under arid environments has been systematically examined in the studies of Charney and his co-workers (Charney, 1975; Charney *et al.*, 1975, 1977) through a biogeophysical feedback model to relate the effect of albedo change on drought in Sahel, Sahara and other semi-arid regions of the world. The premise used in the studies has been appraised as the Charney hypothesis (Williams & Balling, 1996). As to our micro-scale region, the explanation that Otterman (1974) gave for the cause of LST contrast is reasonable but is not enough because it has no quantitative evidence of ground measurements about the difference of albedo and evaporation on both sides. Furthermore, the mechanism leading the LST difference still remains unknown. Actually, LST change of ground surface is controlled by many factors such as subsoil properties including soil thermal conductivity, soil water content and heat capacity. Micrometeorologically and soil-physically, the mechanism leading to LST change is rather complicated. Moreover, the mechanism governing the LST change has not been revealed. Therefore, a study from the viewpoint of micrometeorological modeling is necessary in order to explain the occurrence of the LST anomaly in the region and to understand its implication to desertification.

In this paper, we intend to model the LST change and heat flux variation of the region in terms of surface energy balance. The purpose of this modeling is to understand the mechanism leading to the occurrence of the thermal anomaly and to reveal the key factors controlling the surface temperature change through comparison of surface energy balance dynamics on biogenic crust and bare sand.

Surface energy balance model has been extensively used for various research purposes (Hares & Novak, 1992; Dolman, 1993; Friedl, 1995). A simple surface energy mode was adopted in Dolman & Blyth (1997) to study the behavior of the roughness length of heat and water vapor in heterogeneous terrain. A mathematical model for the numerical computation of evaporation from bare saline soils was presented in Yakirevich *et al.* (1997). In association with remote sensing data, a surface energy balance model was used in Friedl (1996) to examine the issues of land surface properties and heat fluxes over a regional scale. Using remote sensing data as inputs, Schmugge & Humes (1995) applied the surface energy balance model to monitor land surface fluxes. Chen & Coughour (1994) developed a general model for energy and mass transfer of land surfaces by considering the soil temperature change and soil moisture movement separately. The existing studies employed different

methods to simplify the complexity of the model in terms of computation and rarely related soil temperature change to the simultaneous soil moisture movement.

In the study, we intend to establish a complete surface energy balance model that couples soil temperature change simultaneously with soil moisture movement and to develop a methodology for the numerical approximation to the model. Through this model and its numerical solution method, it is possible to estimate surface heat fluxes, surface and soil temperature change, soil water movement and other important micro meteorological parameters that govern surface temperature change without too many assumptions and simplifications to the parts of the model and its parameters. Comparison of surface energy balance performance on the two typical surface patterns of the region will help us to understand the surface temperature difference on both sides of the region. Modeling with the different parameters on these two surface patterns can also reveal the key factors leading to surface temperature difference between the two surface patterns. The mechanism governing the surface temperature difference on the two surface patterns can then be extended to understand the occurrence of the LST anomaly in the desert environment.

Micrometeorological model

Surface temperature in the soil–atmosphere system is determined by a number of micrometeorological and soil-physical factors through the dynamics of surface energy balance. In order to reveal the mechanism leading to the LST anomaly on both sides of the region, it is necessary to establish a micrometeorological model to simulate surface temperature change and heat flux variation of the region from the viewpoint of surface energy balance. Because it is impossible to access the Egyptian side for any field measurement and observation, all the research work has to be done on the Israeli side. Therefore, the simulation is mainly oriented to the two typical surface patterns of the region: biogenic crust representing the Israeli side and the bare sand representing the Egyptian side. According to Qin (1998) and Qin & Kainieli (2000), biogenic crust covers above 72% of the Israeli side and bare sand above 80% of the Egyptian side. Thus, it is reasonable to assume that the LST difference between bare sand and biogenic crust can be extended to represent the general case on both sides of the region. Application of the micrometeorological model to the two surface patterns for comparison of their difference in terms of surface energy balance can finally lead to uncovering of the key factors controlling the sharp LST difference on both sides of the region.

More specifically, the hypotheses based on the micrometeorological modeling for the study can be summarized as follows:

- The difference of surface albedo, which is much higher on the Egyptian side than on the Israeli side, controls the absorption difference of incident global radiation on both sides. Under arid environment, evaporation is minimal due to extremely low soil water content. Thus, the absorption difference of incident energy makes a significant contribution to the difference of LST on both sides. The importance of albedo in the climate change of arid region had been emphasized in several studies (Charney, 1975; Charney *et al.*, 1975, 1977; Cunning & Rowntree, 1986; Williams & Balling, 1996). Our current study intends to examine the importance of albedo difference in leading to the occurrence of the surface temperature contrast across the border.

- The difference of emissivity, which is expected to be lower on the Egyptian side than on the Israeli side, makes a significant contribution to LST difference on both sides of the region. For the same temperature level, emissivity difference determines the energy emitted from the surface, which is observed by remote sensing imagery systems for LST estimation. Higher emissivity means greater ability of emission. And the difference of surface emittance may have a great effect on surface energy balance, which finally shapes the LST difference of the surfaces.
- The difference of subsoil properties especially soil moisture makes a significant contribution to the LST difference on both sides of the region. Surface temperature change strongly relates the change of such subsoil properties as soil heat capacity, thermal conductivity, hydraulic conductivity, soil moisture movement and so on. Alhough the lithological structure of the subsoil on both sides can be viewed as identical, the different process of surface energy balance due to different albedo may also lead to the difference in subsoil properties, which in turn has an important impact on the LST difference on both sides. Studies indicated that soil moisture is very important in shaping regional climate change under arid environments (Cunning & Rowntree, 1986; Lanicci *et al.*, 1987; Williams & Balling, 1996). Thus, the possible difference of soil moisture between the two typical surfaces of the region will also be examined to test their relative role in producing the LST anomaly in the region.

Through the micrometeorological simulation, these hypotheses can be tested on the surfaces of bare sand and biogenic crust. The mechanism leading to the simulation results on the two typical surface patterns can then be extended to understand the surface energy balance for an explanation of LST anomaly on both sides of the region.

The LST change and thermal variation strongly relate to such important environmental factors as sky radiation, wind speed, surface albedo, ground emissivity, soil properties, soil water content, etc. at the interface of land–air system. All of these factors have a significant effect on the LST change and thermal variation on the ground surface. Actually, surface temperature change is a direct reflection of the dynamic energy balance on the surface. For a bare soil surface where energy storage is zero, surface energy balance at the soil–atmosphere interface can be quantitatively described as

$$R_n - H - LE - G = 0 \tag{1}$$

where R_n is the net radiation ($W\,m^{-2}$), H is the sensible heat flux ($W\,m^{-2}$), LE is the latent heat flux ($W\,m^{-2}$), G is the soil heat flux ($W\,m^{-2}$). The terms in Eq in (1) are all related to surface temperature, which becomes the key factor for numerical solution of the model.

The short-wave radiation from the sun is the only energy source driving the dynamics of the interface when there is no heating source from the interior earth. At the ground surface, part of the incident short-wave radiation R_s is reflected by the surface back into the atmosphere at a density that depends on the albedo of the surface. At the same time, the Earth's surface also emits some long-wave radiation into the atmosphere and the atmosphere also emits some long-wave radiation that reaches the ground surface. Some of the incoming atmospheric long-wave radiation is reflected by the ground surface back into the atmosphere. Therefore, the net radiation

can be expressed as (Brutsaent, 1982)

$$R_n = R_s(1-\rho) + \varepsilon_a \sigma T_a^4 - \varepsilon_s \sigma T_s^4 - (1-\varepsilon_s)\varepsilon_a \sigma T_a^4 \quad \text{(Eqn. 2)}$$

where R_n is the net radiation ($W\,m^{-2}$), R_s is the global hemispheric radiation ($W\,m^{-2}$), ρ is the surface albedo, T_s is the surface temperature (K), T_a is the air temperature (K), ε_s and ε_a are the surface and air emissivities, respectively, σ is the Stefan–Boltzmann constant ($\sigma = 5{\cdot}67 \times 10^{-8}\,W\,m^{-2}\,K^{-4}$).

In arid environmental systems, sensible heat flux is the most important term of surface energy balance because it usually accounts for above 3/4 of the net radiation at the interface. There are two key factors that determine the amount of sensible heat flux: temperature difference between the interface and the air near the ground, and the air resistance to heat transfer, which is then strongly related to wind speed near the ground. Thus, the sensible heat flux is usually calculated by the following formula (Verma & Barfield, 1979; Schmugge & Humes, 1995):

$$H = \rho_a c_a (T_a - T_s)/r_a \quad (3)$$

where ρ_a is the density of air ($\rho_a = 1{\cdot}205\,kg\,m^{-3}$ at 20°C), c_a is the specific heat of air (c_a=1005 $J\,kg^{-1}\,K^{-1}$), r_a is the air resistance coefficient to heat transfer ($s\,m^{-1}$), which is given as (Berliner, 1988)

$$r_a = \frac{(\ln(z/z_0) - \varphi_h)}{kU} \quad (4)$$

$$U = \frac{v_z k}{\ln(z/z_0) - \varphi_m} \quad (5)$$

where u_z is the wind velocity ($m\,s^{-1}$) at standard height z (z=2 m), k is the Von Karman constant (k=0·4), z_0 is the roughness length (m) of the surface, φ_h and φ_m are the stability correction parameters for heat and momentum, which can be estimated through the ratio function of standard height to Monin–Obhukov length (Berliner, 1988; Courault *et al.*, 1996).

The energy required for evaporation is generally termed as latent heat flux LE, which can be computed by the following formula (Schmugge & Humes, 1995):

$$LE = 0{\cdot}622L(e_a - e_s)/(P_a(r_a + r_s)) \quad (6)$$

where e_a and e_s are the air and surface vapor pressures (kPa), respectively, P_a is the atmospheric pressure (P_a= 101·325 kPa). L is the latent heat of vaporization (L=2·543 $\times 10^6\,J\,kg^{-1}$), r_s is the surface resistance ($s\,m^{-1}$). Actually, evaporation from the ground surface must be equal to the change of soil water content in the profile. Thus, we have

$$LE - LE_c = 0 \quad (7)$$

where LE_c denotes the energy ($W\,m^{-2}$) caused by the change of soil water content in time interval ∂t. In many cases especially in arid environments, soil water movement over planar directions can be assumed to be negligibly small (Rose, 1979; Brutsaert, 1982). Thus, the energy used for driving soil water movement in time interval ∂t can be computed as follows:

$$LE_c = L \int_0^z \frac{\partial \theta}{\partial t} \mathrm{d}z \quad (8)$$

where t is the time (s) and z is the depth (m) of soil profile under consideration, $\partial\theta/\partial t$ denotes the rate of soil water change. When the planar movement is neglected, the vertical movement of soil water can be described by the following differential equation

(Berliner, 1988):

$$\partial\theta/\partial t = \partial(K_c\partial\psi/\partial z)/\partial z + \partial(gK_c)/\partial z + \partial(hsD_v\partial T/\partial z)/\partial z + \partial(e_vD_v\partial h/\partial z)/\partial z \quad (9)$$

where K_c is the soil hydraulic conductivity ($kg\,s\,m^{-3}$), h is the relative humidity of the gas filled in the soil pore, ψ is the soil water potential ($J\,kg^{-1} = m^2\,s^{-2}$), g is the acceleration due to gravity($g = 9{\cdot}8\,m\,s^{-2}$), s is the slope of saturated vapor pressure *vs.* temperature ($kPa\,K^{-1}$), e_v is the saturated vapor pressure (kPa) and D_v is the apparent vapor diffusivity ($kg\,m^{-1}\,s^{-1}\,kPa^{-1}$). The soil water potential ψ in $J\,kg^{-1}$ is coupled with soil vapor pressure e in kPa and temperature T in K via the equation

$$\psi = RT\,ln(e/e_v) \quad (10)$$

in which R is the universal gas constant ($R = 461{\cdot}52\,J\,kg^{-1}\,K^{-1}$). Actually, soil relative humidity h is calculated as the ratio of soil vapor pressure e and saturated soil vapor pressure e_v, i.e. $h = e/e_v$. Thus, the relationship between soil water potential and relative humidity is given as $\psi = RT\,\ln(h)$. The first two terms of Eqn (9) describe the soil water movement in liquid phase due to potential difference and gravitation, respectively. The last two terms describe the movement of soil water in the vapor phase due to temperature and potential gradients, respectively. Therefore, the change of soil water content with time is described as the function of such important variables as soil water potential, soil relative humidity and soil temperature.

Soil heat flux can be computed from soil temperature change and soil heat capacity in the profile. Usually, soil heat transfer in planar directions is negligibly small and only in the vertical direction is practically worthy of consideration. Thus, the term G in Eqn (1) can be computed as (Kimball & Jackson, 1979)

$$G = \int_0^z C_s \frac{\partial T}{\partial t}\,dz \quad (11)$$

where $\partial T/\partial t$ denotes the rate of soil temperature change and C_s is the volumetric soil heat capacity ($J\,m^{-3}\,K^{-1}$) which can be expressed as $C_s = \rho_s c_s$, in which ρ_s is the soil density ($kg\,m^{-3}$) and c_s the specific heat of soil ($J\,kg^{-1}\,K^{-1}$). However, the specific heat of soil is strongly dependeent on soil properties especially the materials constituting the soil. It is also highly variable, depending on the change of soil water content. Usually, the soil can be viewed as constituted by soil minerals (mainly sand, silt and clay), organic materials, water and air in different proportions. Generally, the specific heat of these soil constituents is stable for practical purposes. Thus, it was suggested that heat capacity of the soil could be computed through the thermal properties of its constituents by linking to their fractions (Marshall & Holmes, 1979; Brutsaert, 1982).

$$C_s = \rho_w c_w V_w + \rho_q c_q V_q + \rho_m c_m V_m + \rho_o c_o V_o + \rho_a c_a V_a \quad (12)$$

where ρ is the density of soil constituents, c is specific heat, V is the volumetric fraction, the subscripts w, q, m, o and a refer to water, quartz, clay mineral, organic materials and air, respectively.

Heat transfer in the soil takes place from the more energetic (hotter) region to those cooler regions where the molecular motion is less energetic (Rose, 1979). At the same time it also causes the imbalance of energy distribution in the soil, which drives soil water movement especially in vapor form in the unsaturated state. And soil water movement also eases the process of soil heat transfer. Thus, a complete description of soil heat flux must consider the equilibrium of these two factors. In the time interval ∂t, the intensity of soil heat transfer can be described by the following differential equation (Berliner, 1988):

$$C_s\partial T/\partial t = \partial(K_s\partial T/\partial z)/\partial z + \partial(hsLD_v\partial T/\partial z)/\partial z + \partial(e_vLD_v\partial h/\partial z)/\partial z \quad (13)$$

where K_s is the soil thermal conductivity ($W\,m^{-1}\,K^{-1}$). The first term on the right-hand side of Eqn (13) describes the heat transfer due to temperature gradient. The second term is the energy due to soil water vapor movement under the temperature gradient. The third term is the energy due to the change of soil water vapor distribution under the gradient of the vapor distribution in the soil.

Numerical solution to the model

The relations in the above surface energy balance model are very complicated. It is impossible to directly express the key factor (surface temperature T_s) of the model as a function of other variables. Usually, to solve such a complicated equation as our model involves the application of a numerical approximation method. Among the approximation methods, the Newton–Raphson iterative technique is a good one because it can rapidly reach the solution with the required accuracy. Since all terms of Eqn (1) are a function of surface temperature (T_s), we can rewrite the equation as

$$f(T_s) = R_n - H - LE - G = 0 \tag{14}$$

which is a successive function within such as interval as $T_s \subseteq (-50^\circ C,\ 100^\circ C)$. Therefore, to apply the Newton–Raphson iterative method for approximation, we start with the point T_s^0 in the interval $T_s^0 \subseteq (-50^\circ C,\ 100^\circ C)$ for the solution of T_s and proceed to determine additional approximation by

$$T_s^{n+1} = T_s^n - \frac{f(T_s^n)}{f'(T_s^n)} \quad (n = 0, 1, 2, \ldots) \tag{15}$$

where $f(T_s{}^n)$ and $f'\ (T_s{}^n)$ are the values of the function $f(T_s)$ and its derivative at $T_s{}^n$. After iterative calculation many times when $\left|f(T_s^n)\right| \to 0$ or is less than the required accuracy, we get $T_s{}^{n+1} = T_s{}^n \to T_s$ and stop the iterative calculation. Thus, we can conclude that $T_s{}^n$ is the solution of surface temperature T_s from the model under the balance of available inputs (Qin *et al.*, 2000).

If dT is taken to be small enough, the derivative $f'(T_s{}^n)$ can be given as

$$f'(T_s^n) = \frac{f(T_s^n + dT) - f(T_s^n)}{dT} \tag{16}$$

To solve the function $f(T_s)$ for T_s also involves the solution of the differential Eqns (9) and (13) simultaneously. The Crank–Nicholson technique can be used to approximate the solution of the two differential equations (Qin *et al.*, 2000).

In order to compute latent heat flux LE for the approximation of surface temperature T_s, Eqn (7) also has to be solved for vapor pressure e_s or relative humidity h_s of the ground surface. Both LE and LE_c can be viewed as the function of h_s and Eqn (7) can similarly be solved using the Newton–Raphson iterative approximation method. The procedure of the solution is the same as that used for the solution of T_s from Eqn (14).

The use of Newton–Raphson approximation to solve surface temperature and latent heat flux from Eqns (1) and (7) involves the solution of differential Eqns (9) and (13). Using the relation between water potential and relative humidity, we can rewrite Eqn (9) as

$$C_h \partial h/\partial t = \partial(K_a \partial T/\partial z)/\partial z + \partial(K_b \partial h/\partial z)/\partial z + g\partial K_c/\partial z \tag{17}$$

where the parameters are defined as follows:

$$C_h = (\partial\theta/\partial h) \tag{18}$$

$$K_a = RK_c \ln(h) + hsD_v \tag{19}$$

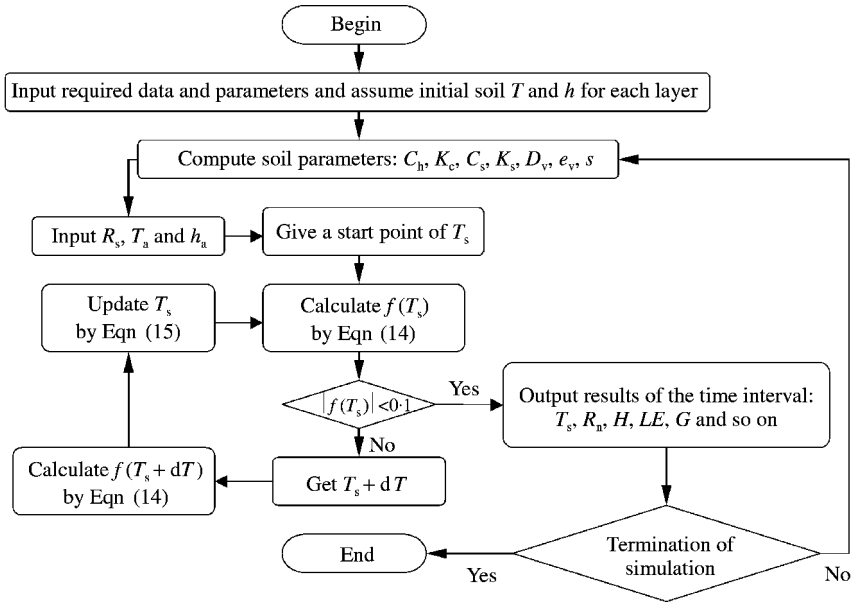

Figure 3. The main flow chart of the model's computation.

$$K_b = RK_cT/h + e_vD_v \tag{20}$$

Similarly, differential Eqn (13) can be reorganized as

$$C_s\partial T/\partial t = \partial(K_d\partial T/\partial z)/\partial z + \partial(K_e\partial h/\partial z)/\partial z \tag{21}$$

where K_d and K_e are defined as

$$K_d = K_s + hsLD_v \tag{22}$$

$$K_e = e_vLD_v \tag{23}$$

Eqns (17) and (21) cannot be solved except when the initial and the boundary conditions are given. For the time node $j+1$, we can use the value of time node j for the initial conditions. Thus, at the beginning, an initial condition is generally assumed for the solution. And after the value of $j+1$ is computed, we use it as the initial condition for the next iteration of computation until modeling termination (Fig. 3).

It is a fact that soil temperature and soil water content remain constant at specific depth from the surface (Brutsaert, 1982; Kutilek & Nielson, 1994) during the time considered such as days. Thus, the constant value of soil temperature and water content at that depth can be used as lower boundary conditions T_n and θ_n of Eqns (17) and (21). The upper boundary of the soil temperature and soil water content for time node $j+1$ is usually determined by considering a small change to the surface temperature and surface water content for time interval j.

A theoretical solution to the differential Eqs (17) and (21) is extremely difficult due to many implicit relations. Usually, the differential equations can be solved through an explicit approximation method but the explicit method is only valid (i.e. convergent and stable) for $\delta t/\delta z^2 \leqslant 1/2$, in which δt is the time interval and δz the depth of soil layer (Smith, 1978). Considering the dimension of time in seconds and depth in meters, the explicit method will create a giant computation volume for a short period

of simulation such as one day. For example, if $\delta z = 0{\cdot}1\,\mathrm{m}$, the time interval has to be $\delta t \leqslant 0{\cdot}005\,\mathrm{s}$ in order to meet the convergent condition of the method. Consequently, it takes about 200 iterative computations for the simulation of 1 s. Crank & Nicolson (1947) developed a method that reduces the total volume of calculation and is valid for all finite values of $\delta t/\delta z^2$ such as $\delta t = 60\,\mathrm{s}$ and $\delta z = 0{\cdot}01\,\mathrm{m}$. They approximated the differentials by the mean of its finite-difference representations on the $(j+1)$th and the jth time node. Applying this implicit method, the differential Eqn (17) can be approximated as follows:

$$\begin{aligned} -K_{ai-1/2,j}T_{i-1,j+1} + (K_{ai-1/2,j} + K_{ai+1/2,j})T_{i,j+1} - K_{ai+1/2,j}T_{i+1,j+1} - K_{bi-1/2,j}h_{i-1,j+1} \\ +(K_{bi-1/2,j} + K_{bi+1/2,j} + 2Z_iC_{hi+1/2,j})h_{i,j+1} - K_{bi+1/2,j}h_{i+1,j+1} = g_j \end{aligned} \tag{24}$$

where $Z_t = \delta z^2/\delta t$ and

$$\begin{aligned} g_j =& 2Z_tC_{hi+1/2,j}h_{i,j} + K_{ai+1/2,j}(T_{i+1,j} - T_{i,j}) \\ & - K_{ai-1/2,j}(T_{i,j} - T_{i-1,j}) + K_{bi+1/2,j}(h_{i+1,j} - h_{i,j}) \\ & - K_{bi-1/2,j}(h_{i,j} - h_{i-1,j}) + 2dzg(K_{ci+1,j} - K_{ci,j}) \end{aligned} \tag{25}$$

Similarly, approximation of Eqn (21) leads to

$$\begin{aligned} -K_{di-1/2,j}T_{i-1,j+1} + (K_{di-1/2,j} + K_{di+1/2,j} + 2Z_tC_{si+1/2,j})T_{i,j+1} - K_{di+1/2,j}T_{i+1,j+1} \\ -K_{ei-1/2,j}h_{i-1,j+1} + (K_{ei-1/2,j} + K_{ei+1/2,j})h_{i,j+1} - K_{ei+1/2,j}h_{i+1,j+1} = G_j \end{aligned} \tag{26}$$

where G_j is defined as

$$\begin{aligned} G_j = 2Z_tC_{si+1/2,j}T_{i,j} + K_{di+1/2,j}(T_{i+1,j} - T_{i,j}) - K_{di-1/2,j}(T_{i,j} - T_{i-1,j}) \\ +K_{ei+1/2,j}(h_{i+1,j} - h_{i,j}) - K_{ei-1/2,j}(h_{i,j} - h_{i-1,j}) \end{aligned} \tag{27}$$

In Eqns (24) and (26), soil temperature T and relative humidity h for time node j are known as initial conditions and the coefficients K_a, K_b, K_d and K_e can be computed for j. Thus, g_j and G_j are also known. For $j+1$, the upper boundary $T_{0,j+1}$ and $h_{0,j+1}$ and the bottom boundary $T_{n+1,j+1}$ and $h_{n+1,j+1}$ are also given. Therefore, the expansion of Eqn (24) about soil water movement in terms of relative humidity will result in the following simultaneous equations:

$$\begin{aligned} +b_1T_1 - c_1T_2 + e_1h_1 - f_1h_2 &= g_1 \\ -a_2T_1 + b_2T_2 - c_2T_3 - d_2h_1 + e_2h_2 - f_2h_3 &= g_2 \\ &\cdots \\ -a_iT_{i-1} + b_iT_i - c_iT_{i+1} - d_ih_{i-1} + e_ih_i - f_ih_{i+1} &= g_i \\ &\cdots \\ -a_nT_{n-1} + b_nT_n - d_nh_{n-1} + e_nh_n &= g_n \end{aligned} \tag{28}$$

Similarly, Eqn (26) about the soil temperature change can also be expanded as

$$\begin{aligned} +B_1T_1 - C_1T_2 + E_1h_1 - F_1h_2 &= G_1 \\ -A_2T_1 + B_2T_2 - C_2T_3 - D_2h_1 + E_2h_2 - F_2h_3 &= G_2 \\ &\cdots \\ -A_iT_{i-1} + B_iT_i - C_iT_{i+1} - D_ih_{i-1} + E_ih_i - F_ih_{i+1} &= G_i \\ &\cdots \\ -A_nT_{n-1} + B_nT_n - D_nh_{n-1} + E_nh_n &= G_n \end{aligned} \tag{29}$$

Totally, there are $2 \times n$ unknown variables and $2 \times n$ equations in Eqns (28) and (29).

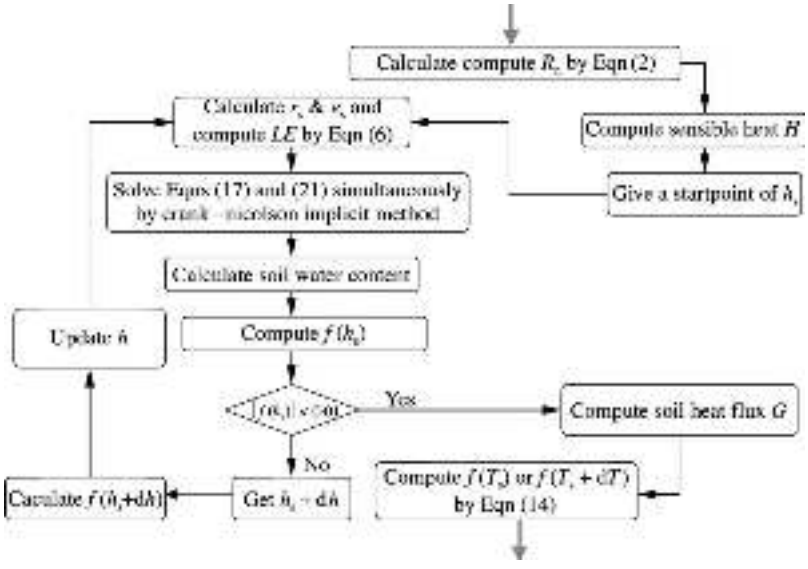

Figure 4. The flow chart for computing $f(T_s)$ and $f(T_s+dT)$.

Thus, the unknown variables can be directly solved from the equation system by Gauss's elimination method (Qin *et al.*, 2000).

The numerical approximation to the model involves the re-adjustment of some given parameters in the iterative calculation. The computation is actually rather complicated. The procedure involves several iterations and the actual computation, as we can imagine, is very complicated. Using Quick BASIC 4·5, we have programmed the model for practical application. The main flow chart of the computation of the model is illustrated in Fig. 3 and the flow chart for computing $f(T_s)$ and $f(T_s+\delta T)$ in Fig. 4.

Data for the modeling

In order to apply the model to simulate LST change and thermal variation on both sides of the region, we need to prepare the required data sets of the functioning factors for its operation and computation. These include global radiation, surface albedo, soil water content, air temperature, relative humidity of the air and wind speed near the surface.

Global radiation of the region

The observed LST anomaly on both sides of the border region has the sharpest appearance in the summer season, which is dry and hot. This implies that our simulation should focus on the season. The global radiation of the region was measured during July 16–20, 1998, when the sky was very clear and the region was very dry and the vegetation was dormant. The global radiation was measured with a pyranometer operating in the spectrum ranging from ultraviolet through visible to near-infrared wavelength. Thus, the measurement is a full spectrum measurement of the global radiation. The pyranometer was mounted upward on top of a frame 1 m

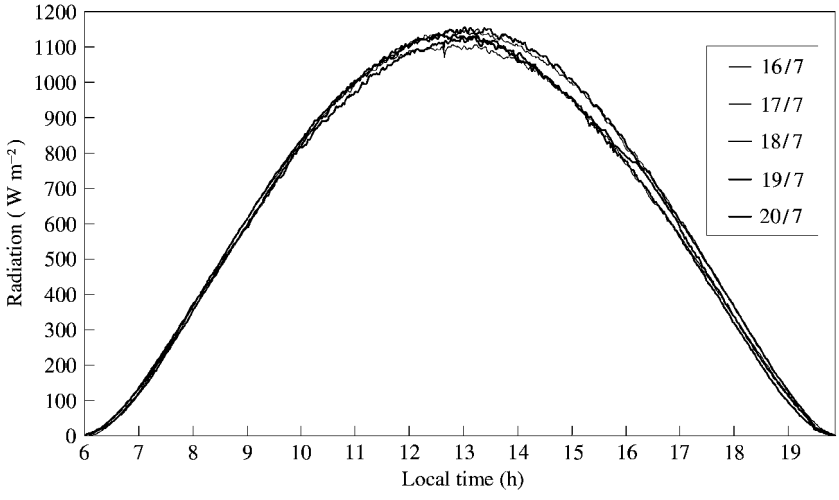

Figure 5. Global radiation of the region measured on July 16–20, 1998.

above the ground, which was carefully installed so that it is in the water level status to record the radiation from the hemispheric direction. A datalog and a storage module were used to record the data from the pyranometer at a frequency of every 5 s for one record. The raw data were averaged to one record for each minute after download into the computer for further calculation.

The measuring results are shown in Fig. 5, indicating the global radiation change during the measuring period and their average. The global radiations during the measuring period are very similar to each other. The shape of the radiation curves has perfect similarity with a sine one. The curves started from a little bit earlier than local time 6:00 at dawn and ended at 19:45 at dusk, representing the period when the region receives the incoming radiation for its surface energy balance process. From 6:00 in the morning, the radiation rapidly increases with time, due to the increase of the sun's shining angle. At about 13:00 when the sun's rays are about perpendicular to the ground, the radiation curves reach their apex and from this point to about 17:45 at dusk, the radiation declines gradually. At the apex hour 13:00, the global radiation of the region is about $1130\,\mathrm{W\,m^{-2}}$ on an average during the measuring period. Another feature of the radiation curves is that the fluctuation in the morning is much less than that in the afternoon. During the measuring period, the daily change of the radiation is less than $15\mathrm{W\,m^{-2}}$ from 6:00 a.m. to 11:00 a.m. However, the change in the afternoon is above $35\mathrm{W\,m^{-2}}$. For a specific day, the fluctuation is much more obvious in the noon hours than the other ones. After average, the curve is very smooth in the morning and afternoon except for a little bit of fluctuation in the noon hour from 12:30 to 13:30. Therefore, we can conclude that our measurement produces a good result of global radiation measurement of the region.

Albedo of the surface patterns

Albedo is defined as the ratio of reflected radiation to the incident radiation. In order to calculate the albedo of ground surface, we need to measure the reflected radiation and the incoming radiation simultaneously. The two pyranometers were mounted at a frame about 1 m from the ground. One pyranometer was placed upward to measure

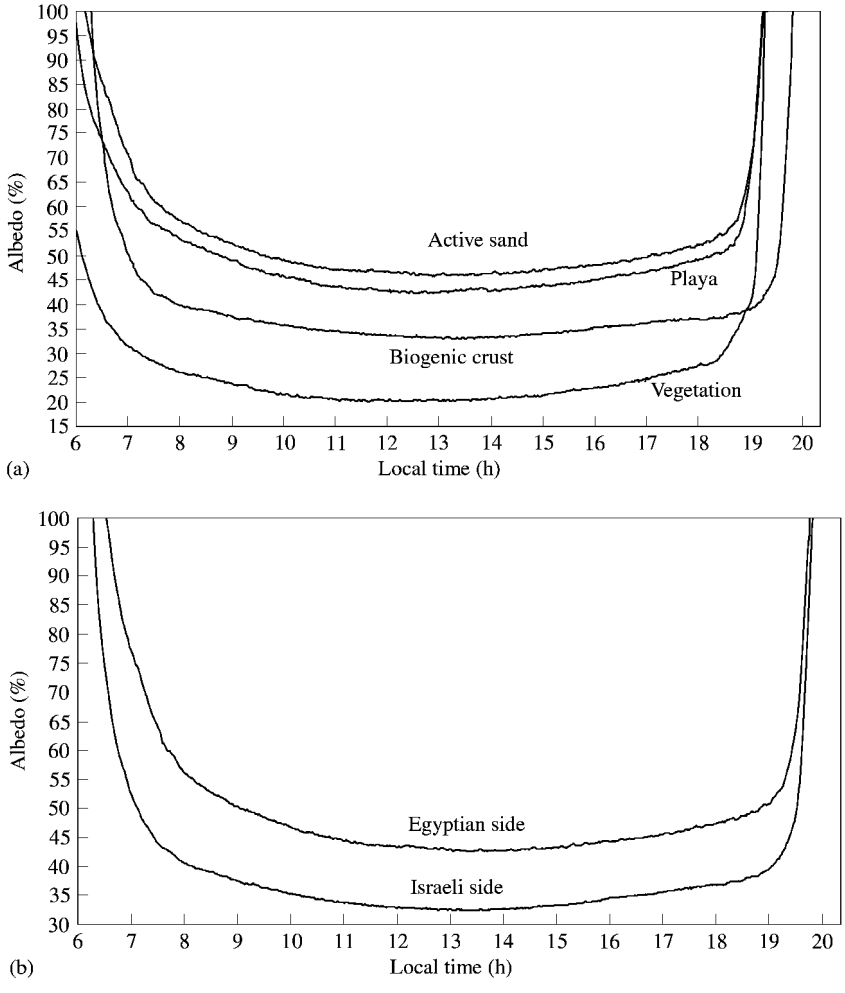

Figure 6. Albedo of (a) main surface patterns as well as (b) the Israeli side and the Egyptian side.

the incoming (downward) radiation of the sky and the other downward to measure the reflected radiation from the ground. Both the pyranometers must be kept at the water level. The measuring period was the same as the radiation measurements. Before calculating the albedo, the data from the two pyranometers were calibrated into a common level so that the measurement errors could be minimized. In practice, we use the pyranometer recording the incoming radiation as base level and to calibrate the pyranometer recording the reflected radiation into the base level.

The average albedo of the typical surfaces is shown in Fig. 6(a), which indicates the change of surface albedo with time during the day. One obvious common feature of the albedo change is that its amount declines with increase of solar angle. Usually, the sun's rays are perpendicular to the ground at about noon (13:00 local time). Therefore, the albedo of the surfaces is minimum around this time (13:00–14:00). Actually, the NOAA–AVHRR also passes the region at about 14:00. That is, when the NOAA–AVHRR remotely scans the region, the albedo is at the lowest level. The albedo of all surface patterns is extremely high at dawn and dusk. At this time, the

azimuth angle of the sun's rays is very small and the reflected fraction of the incident radiation is very high, though both the incoming and reflected radiations are very small ($<50\mathrm{W\,m^{-2}}$).

The albedo of the four surface patterns also show great difference. In the hours around noon, the sand surface has the highest albedo, followed by playa, then biogenic crust. Desert shrub has the lowest albedo. The albedo difference between sand and playa is very small, only about 2–5%. However, the difference is very obvious between sand and biogenic crust. During the noon hours, biogenic crust has an albedo of about 33%, which is 13% lower than that of sand surface and 10% lower than playa. Sand and biogenic crust constitute the overwhelming surface composition on both sides of the region (Karnieli *et al.*, 1996; Qin, 1998; Qin & Karnieli, 2000). The great difference of albedo between sand and biogenic crust would surely make an extremely important contribution to the difference of surface temperature on both sides.

Using the surface composition given in Qin & Karnieli (2000), we are also able to estimate the average surface albedo for both sides. The result of such an effort is shown in Fig. 6(b). Due to the higher percentage of biogenic crust and vegetation, which have lower albedo, the Israeli side has much lower surface albedo than the Egyptian side. At about noon, the average albedo on the Israeli side is about 32%, which is about 12% lower than that on the Egyptian side. This difference is critical in shaping the dynamics of surface energy balance on both sides.

Soil water content

In arid and semi-arid environments, the importance of soil moisture or soil water content in driving the dynamics of climate phenomenon has been well known (Lanicci *et al.*, 1987; Williams & Balling, 1996). Water content of soil profile is needed for the simulation in two ways: (1) determination of initial and boundary conditions for the solution of differential equations about soil water movement and temperature change, and (2) validation of simulation result about soil water movement in the region. Generally, soil water content can be determined by several methods (Ghildyal & Tripathi, 1987; Gardner *et al.*, 1991; Kutilek & Nielson, 1994). When suitable instruments such as neutron moisture meter are available, soil water content can be easily measured in the field by installing the probe at various depths of soil profile (Marshall & Holmes, 1979). For our study, we lack the instrument for direct measurement. Thus, we have to use the classic gravimetric method of drying soil samples for the measurement. Actually, soil water percolation and movement of the sand dunes had been studied in the research of Yair *et al.* (1997), who used neutron probes to monitor soil water content change for the analysis in the rainfall years 1991–1992 and 1992–1993. Soil water content data of the region in recent years are not available and the comparison of soil water content under sand and biogenic crust surfaces also still remains not to be done.

In order to obtain soil moisture data of the region, a series of samplings had been conducted for measuring soil water content under sand and biogenic crust surfaces. The sampling period ranged from the rainy season to the dry hot one in 1998. All soil samples were taken from the field at the Nizzana Research Site on the Israeli side (see Fig. 1). The results are presented in Fig. 7.

After heavy rain, soil water content is much higher in the profile under biogenic crust than under sand surface. According to the sampling on January 25, which was about 2 weeks after heavy rain (23·9 mm) on January 11–12, soil had about 18% volumetric water content under biogenic crust and 10% under bare sand surface. Water penetration in the soil of the region seems to be very slow. Within 1 week after heavy rain, the soil below 40 cm was still very dry under sand surface (Fig. 7(a)). After 2 weeks, the water finally penetrated into its maximal depth.

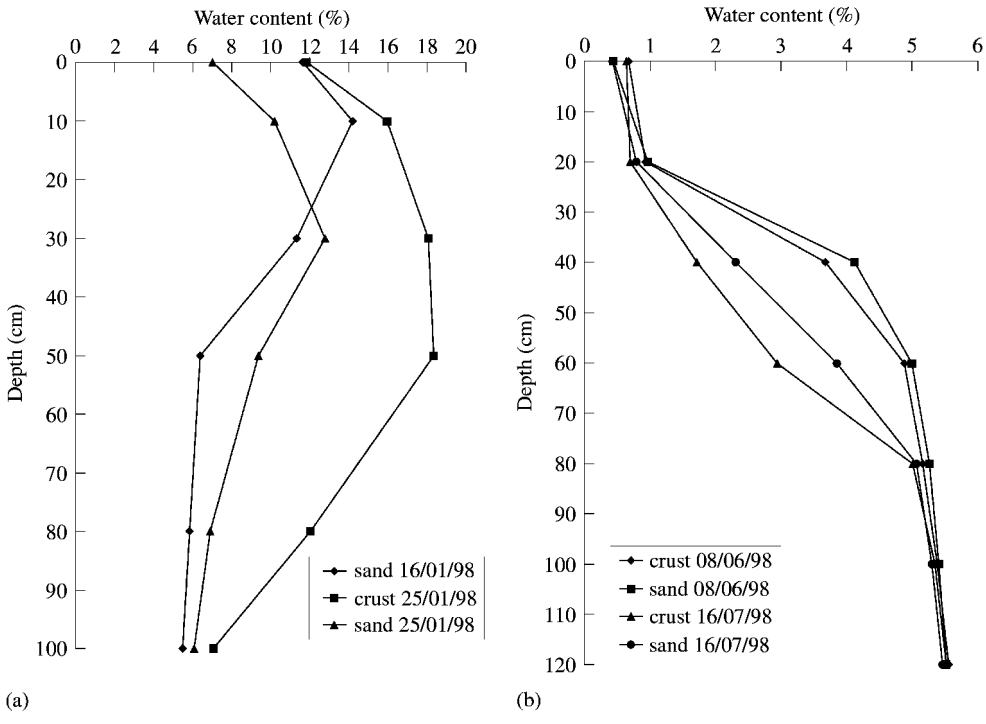

Figure 7. Comparison of volumetric soil moisture content under biogenic crust and bare sand surfaces in (a) wet season and (b) dry season.

In the summer season, the region is very dry. Soil water content in the surface layer is only about 0·5–0·8%. One interesting phenomenon is that the upper layer has a little bit higher soil content under biogenic crust than bare sand surface though the difference is very weak due to both being extremely low. However, the lower layer of soil profile under sand surface may have higher soil water content than that under biogenic crust surface. Soil water content may reach 2·31% at 40 cm under sand surface, which is about 0·5% greater than that under biogenic crust, according to the sampling on July 16, 1988. This difference is probably due to different speeds of the soil water attenuation in the two soil profiles.

It seems that seasonal rain only affects the soil water change of the top 1 m profile. Soil water content tends change little at the layers below 1 m in the wet season and below 0·8 m in dry the season. At this depth, the soil water content is about 6–7% in the wet season (Fig. 7(a)) and 5·0–5·5% in the dry season (Fig. 7(b)). Similar results had also been reported in Yair *et al.* (1997).

Soil moisture data of the region need to be carefully set for the simulation. From the above sampling results, we can see that the surface is extremely dry in the hot summer and the soil profile loses its water content rapidly after the rains. In the dry hot season, the surface contains not more than 1% of volumetric soil water content in both sand and biogenic crust. Under about 80–100 cm, the soil water content may reach up to 5·0–5·5% and it seems that the change below this depth is negligibly small. Therefore, this content can be used as the lower boundary soil water content for the solution of our model. It should be noted that the soil water content under the two surface

patterns is different. The content under sand surface is slightly higher than that under biogenic crust. Usually, the former has about 0·5–0·7% volumetric soil water content at about 40 cm depth than the latter and at 60 cm depth the difference may be up to 1%. This difference may have an important impact on the contrast of surface temperature change on both patterns.

Air temperature and relative humidity

The meteorological data of air temperature and relative humidity were measured at 2 m above the ground at the Nizzana Research Site on the Israeli side (see Fig. 1) in July 1998, which represents the hot dry summer season of the region.

The average air temperature change has been plotted in Fig. 8(a). Although there are fluctuations in the curves, the general trend of the change can be clearly seen. No obvious differences of average air temperature can be found in all 10 days of July 1998. The average air temperature of the region reaches high level of up to about 36°C at early afternoon (14:00–15:00). Minimum air temperature occurs at about 5:00–6:00 when the temperature is in the range of 20–23°C (Fig. 8(a)). Thus, daily air temperature vibration of the region is up to 13–15°C. Air temperature increases sharply in the morning and decreases quickly in the afternoon. After midnight, air temperature undergoes a very slow change. This represents the typical meteorological feature of arid environments. Because air temperature change is relatively identical, the average of the whole month will be used as the input of our modeling.

The average change of air relative humidity is shown in Fig. 8(b). Relative humidity not only relates to water vapor pressure but also depends on air temperature. When the air temperature is high, relative humidity is low. This explains the fact that the change in the relative humidity is opposite to the change in air temperature. During the night, air temperature is low but the relative humidity is high while during the day the air temperature increases which leads to the decrease of relative humidity. Minimal air humidity occurs at about 14:00, when it is only about 30–40%. Maximal humidity exists in the hours 2:00–5:00, when it may reach up to 85–95%.

Wind speed and roughness length

Wind speed is an important factor in micrometeorological modeling (Diak & Whipple, 1993; Dolman, 1993). The connection of wind speed to surface temperature change is that it directly affects the amount of sensible and latent heat fluxes which control the cooling process of the surface. The greater the wind speed, the smaller the air resistance for sensible heat transfer into the air. Wind speed data of July 1988 are available for the analysis of its daily change as shown in Fig. 9. Several features can be seen in Fig. 9. First of all, there is a peak in the late afternoon when wind speed is observed to be maximal. The peak is between 16:00 and 18:00 in July (Fig. 9). The value of wind speed during the hours is about $4{\cdot}8\,\mathrm{m\,s^{-1}}$. Second, wind speed is generally greater in daytime than at night-time. After reaching the peak in the late afternoon, wind speed quickly declines in the evening. Figure 9 indicates that the speed drops to the minimum (about $1\,\mathrm{m\,s^{-1}}$) at midnight. In summer, the ascent of wind speed accelerates in the late morning hours during the day till late afternoon at about 17:00. Third, the difference between daytime maximum and night-time minimum is about $4{\cdot}5\,\mathrm{m\,s^{-1}}$. Fourth, due to the spatial variation of geomorphological shapes of the region, a periodical cycle of regularity is clear in the daily wind speed change under general governance of local meteorological conditions. The average wind speed will be used as the input data of our modeling.

Due to the importance of roughness length in energy balance models for evaporation estimation, many studies have been carried out for the determination of

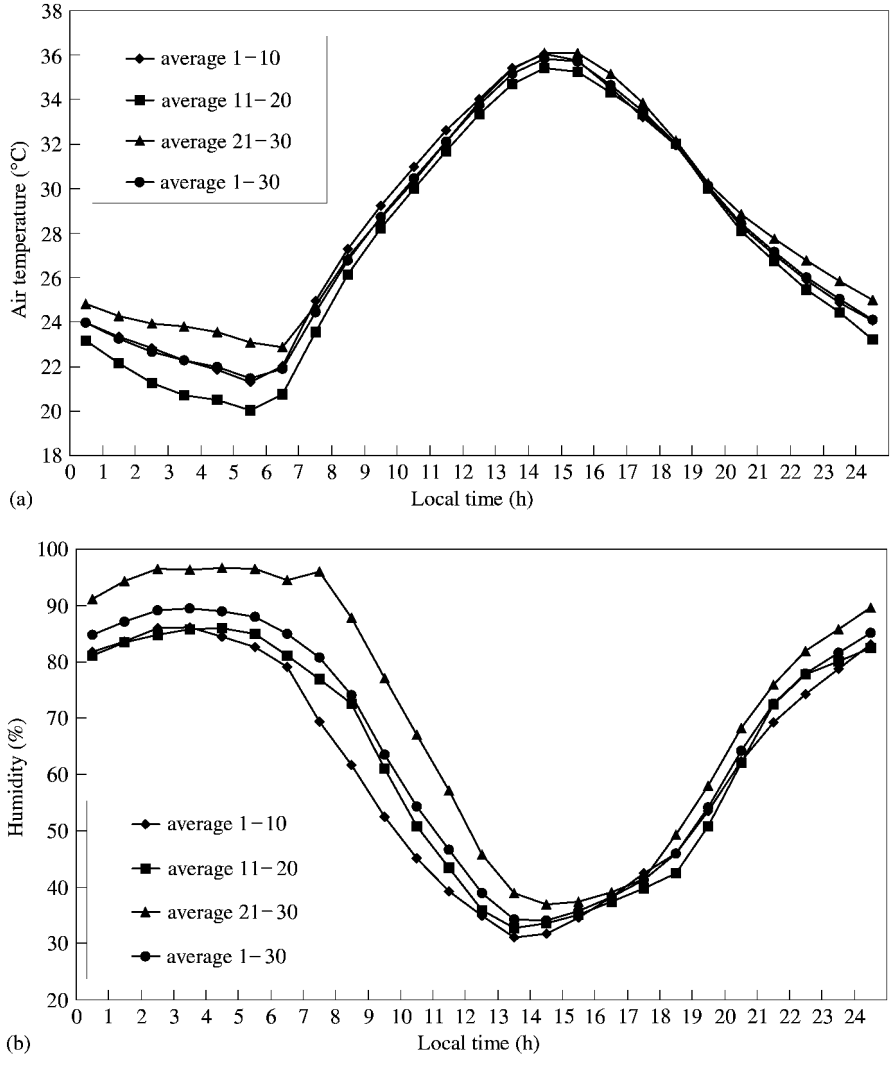

Figure 8. Daily change of (a) air temperature and (b) relative humidity of the region in July 1998 (Based on the measurements of Dr. Thomas Litmann).

this parameter under various situations (Monteith, 1973; Brutsaert, 1982). The magnitude of this parameter strongly depends on the surface conditions. Specifically, it has a close correlation with the height (h) of vegetation. Choudhury *et al.* (1986) calculated this parameter for wheat as $z_0 = 0{\cdot}13h$, where h is the height of wheat in their study. Szeicz *et al.* (1969) found that roughness length on fully developed maize and sorghum for wind speeds of approximately $2.5\,\mathrm{m\,s^{-1}}$ was $0{\cdot}105h$ and Garratt (1984) stated that $0{\cdot}1h$ could be a rough estimation of z_0 though its range can vary from $0{\cdot}02h$ to $0{\cdot}2h$. Based on their data, van Bavel & Hillel (1976) reported a roughness length of $z_0 = 0{\cdot}01\,\mathrm{m}$ for bare soil in an open area. After reviewing the literature of relevant studies, Brutsaert (1982) gave a proportion of $z_0 = h/8$ for a broad range of vegetation types.

As to our study region, the surface is mainly covered with some shrubs with a height of less than $0{\cdot}5\,\mathrm{m}$. Therefore, according to the proportion given by Brutsaert (1982),

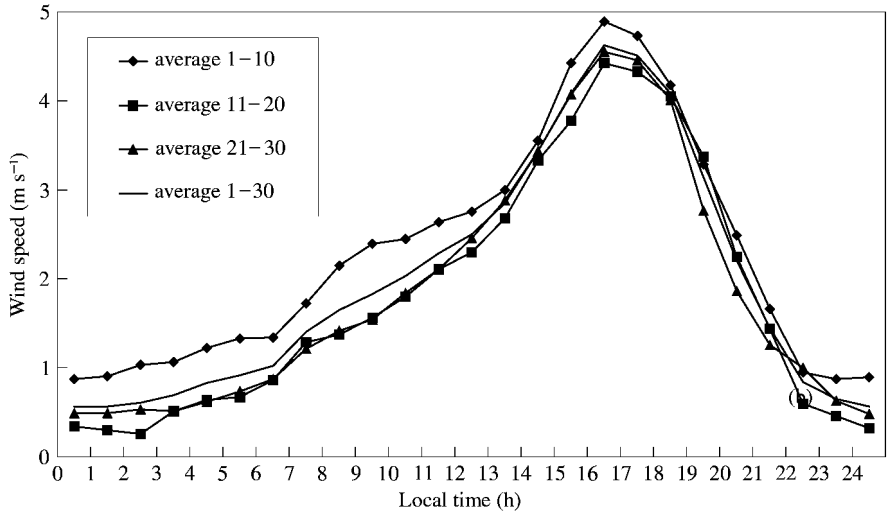

Figure 9. Wind speed of the region in July 1998 (Based on the measurements of Dr. Thomas Litmann).

we get $z_0 = 0{\cdot}062$ m. Based on the rough estimation of Garratt (1984), we have $z_0 = 0{\cdot}05$ m. Please note that this proportion is for the dense vegetation types. The sand dune region is an arid desert and shrub only occupies about 17·5% of the surface on the Israeli side and about 4·5% on the Egyptian side (Qin, 1998). The situation of vegetation type in the sand dune region is far from those assumed for the proposed proportion of the parameter to the height. Thus, we can conclude that the parameter in the sand dune region is between the bare soil ($z_0 = 0{\cdot}01$ m) and the dense vegetation ($z_0 = 0{\cdot}05$ m). Considering the vegetation density of the region, we employ $z_0 = 0{\cdot}02$–$0{\cdot}03$ m for our modeling.

Simulation results and analysis

The purpose of the simulation is to compare the difference of daily performance of surface temperature change and heat flux variation on the two most important patterns (bare sand and biogenic crust) and to distinguish the leading factors governing the difference. An analysis of the simulation results can help us to understand as to why there is a significant surface temperature difference on both sides of the region and what factors contribute more to the difference than others.

Modeling LST change of biogenic crust and active sand

Simulation of surface temperature change was carried out for two data sets: one for biogenic crust and one for bare sand surface. Therefore, all required parameters are carefully designed according to the two surface patterns. Fortunately, the soil (fine sand) under the two surfaces is similar due to the same soil formation process in the region. This provides an easy way of preparing soil property data for the simulation. The data sets required for the modeling have been described in the previous section.

According to the situations of the region and due to the extreme scarcity of knowledge about the micrometeorological change and soil physics of the Egyptian side, several assumptions have been constructed for the simulation. First of all, some

meteorological indicators such as global radiation, air temperature, air humidity and wind speed near the surface are assumed to have little variation on both sides of the region due to the spatial adjacency. This may not be true, especially for air temperature, air humidity and wind speed. Usually, air temperature is strongly related to the surface temperature and wind speed is due to the air temperature difference. Since the Israeli side is observed to be hotter, its air temperature should be higher than the Egyptian side. However, the assumption of similar air temperature on both sides will allow us to focus our simulation on the variation of soil properties and surface features for explaining and understanding the LST anomaly of the region. Actually, as we will see in the following simulation results, the simulated surface temperature difference with identical air temperature is slightly lower than the actually observed one. This means that the differences of air temperature, wind speed and air humidity also have some effects on the difference of surface temperature. However, their relation with surface temperature is mutually dependent. Thus, in order to reveal the actual factors that lead to the occurrence of the thermal anomaly across the border, it is better to isolate the functioning of these mutually dependent factors by assuming the same values for them in the modeling.

Second, surface temperature change on the Israeli side can be represented by the thermal performance of biogenic crust due to the fact that more than 72% of its ground surface is covered with the surface pattern (Qin & Karnieli, 2000). The Egyptian side can also be represented by bare sand because of its surface constituents. The surface in the real world is in fact a mixed one composed of several patterns. Simulation through surface energy balance equation requires a specific data set for the surface under consideration. For a mixed surface, some soil parameters such as soil constituent fraction are really difficult to properly estimate through surface composition. Therefore, the way to analyse the surface temperature change on both sides is through comparison of thermal variation of the two typical surface patterns.

Third, the lower boundary conditions of soil profile for solving the soil heat transfer equation and soil water movement equation are assumed to be the same for the two typical surface patterns. No daily change of soil temperature and soil water content is assumed at about 0·5 m from the surface. Actually, daily heat penetration into the soil is within 30–50 cm depth in an arid environment (Hausenbuiller, 1978). According to the reports of Fania & Zipora (1997) and Zemel & Lomas (1977) who monitored soil temperature regime in Israel, the assumption of no daily soil temperature change at about 50 cm depth is reasonable for the south Israeli desert environment.

Performance of daily surface temperature change on the two surfaces

The most important output of the modeling is the LST change of the two surfaces under consideration. The simulated daily surface temperature change of bare sand and biogenic crust in the dry summer season is shown in Fig. 10(a). In order to have a reference for comparison, the real average air temperature change is also plotted in the figure, from which several features can be clearly identified. First of all, the surface temperature of biogenic crust and bare sand surface in the summer season can reach as high as 48–50°C at about noon when temperature peak occurs. The range of the change is quite well corresponded to the observed change through ground truth measurements and on remote sensing images (Qin *et al.*, 2000). Note that the data used for the simulation represent the general situation in the summer season and are measured at the Nizzana Research site on the Israeli side, which is adjacent to the border. Thus, the simulation result based on the data only reveals the general or the average change of surface temperature of the two surfaces in the area adjacent to the border. This does not deny the possible higher or lower performance of the surface

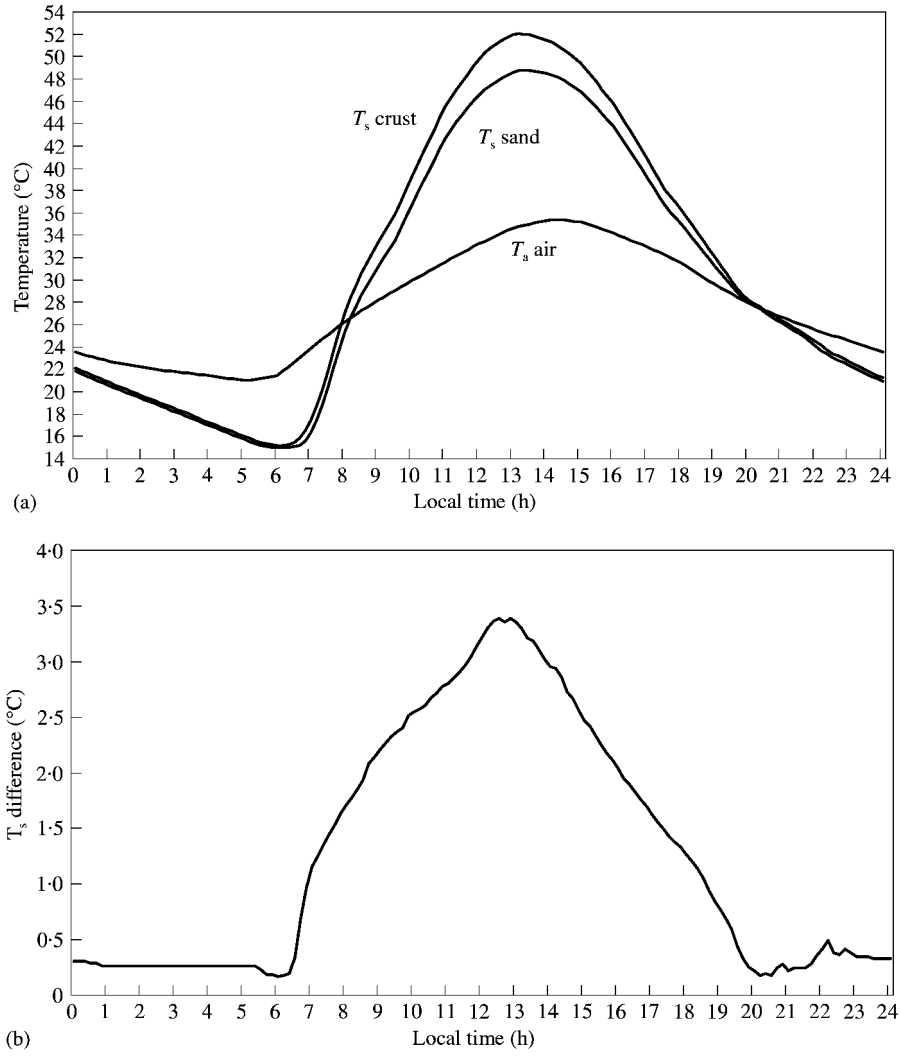

Figure 10. Comparison of daily surface temperature fluctuation on biogenic crust and sand surfaces, illustrating (a) LST change of the two surfaces and (b) LST difference between the two surfaces.

temperature peak on a specific day under specific conditions such as in the area far from the border on the Israeli side, where very high LST can be found (see Fig. 2).

Second, the surface temperature of biogenic crust is higher than that of bare sand surface during the daytime and the difference between the two surfaces disappears during the night. The daytime surface temperature difference on the two surfaces is clearly shown in Fig. 10(b), from which we can see that the maximal difference of LST between the two surface patterns is up to 2·8°C at about noon, which is slightly lower than the actually observed difference (generally >3°C) between the two surfaces (Qin *et al.*, 2000). This implied that biogenic crust is much hotter than bare sand under the beaming of strong solar radiation in summer when little soil water is available for evaporation. However, the night-time difference of surface temperature change between the two patterns is not obvious. This change of daytime and night-time LST

difference is extremely important in the explanation of thermal variation on both sides of the region. The phenomenon of LST difference is observed to be obvious during the daytime at about 14:00 *in situ* satellite pass but this temperature difference is very obscure on night-time image of remote sensing (Fig. 2(b)). More important is the fact that the simulated surface temperature at about midnight is about 22°C (Fig. 10(a)) and the sharp LST contrast tends to disappear at this temperature level.

Third, the surface temperature of biogenic crust and bare sand is much higher than air temperature during the daytime and is much lower than air temperature during the night-time. This is in accordance with the general situation of temperature change in an arid environment. Generally speaking, daytime in an arid environment is very hot and night-time is cool. Daily variation of air temperature is up to 15°C and that of surface temperature is even higher (up to 35°C).

Fourth, the surface temperature increases rapidly in the early morning and declines rapidly in the late afternoon. The minimal surface temperature can be seen in the early morning at about 5:00 when it is about 15°C. The surface temperature starts to ascend from 6:30 and its maximal ascendance can be seen in the hours from 7:00 to about 9:00. During this period, it climbs rapidly from about 16°C to 33°C. In the afternoon, rapid descent of surface temperature occurs in the hours from 16:00 to about 19:00. It drops from about 42°C to 27°C. This change reveals the general warming and cooling process of the region in the hot dry summer season.

Sensitivity analysis of the modeling

The parameters for sensitivity analysis are the important ones that govern the surface temperature change of the region. Totally, 22 parameters are selected to test the sensitivity of the modeling. These parameters and the result of the sensitivity analysis are listed in Table 1.

What we are concerned with is the modeling of the surface temperature change under the governance of these parameters. Thus, the sensitivity analysis of the modeling is to test the change of surface temperature with the small change of these parameters. The output of the modeling for the data set of biogenic crust surface is used as the reference of comparison for the sensitivity analysis. Because we are more interested in the change of surface temperature in the early afternoon when satellite passes, the average surface temperature at 12:00–14:30 is used as the reference of surface temperature for the analysis. As to the small change of the parameters, we define it as 1%. Thus, for a specific parameter, the aim of the analysis is to answer the following question: how many percents of surface temperature change would result from the change of 1% in that parameter under consideration?

Table 1 indicates that the largest change in T_s is observed for a small change in air temperature and global radiation. When air temperature increases by above 1% (about 0·36°C), the average surface temperature will increase by about 0·345°C, with 0·749%. Since air temperature and surface temperature are mutually dependent, we expect that the actual higher air temperature exists on the Israeli side, which consequently exacerbates the surface temperature difference across the border. An increase of 1% in global radiation will result in 0·128°C increase in surface temperature, with 0·278%. Actually, air temperature and global radiation are the two essential factors of the modeling. Global radiation determines the amount of energy available for the micrometeorological and hydrological process in the soil–air interface system. And air temperature governs the exchange of energy between the ground and the air, and is the result of the exchange as well. Their sensitivity to LST change in the modeling implies their importance in the simulation.

A 1% increase in surface albedo, roughness length and surface emissivity corresponds, respectively, to a decrease of 0·059°C, 0·043°C and 0·022°C in surface

Table 1. *Sensitivity analysis of the simulation model*

Parameters	Change of T_s in °C	Change of T_s in %
Roughness length	−0·04287	−0·09302
Surface emissivity	−0·02166	−0·04699
Surface albedo	−0·05914	−0·12831
Soil thermal conductivity: quartz	0·00138	0·00300
Clay minerals	0·00144	0·00313
Soil air	−0·00272	−0·00589
Soil composition: quartz	0·00294	0·00638
Clay minerals	0·00631	0·01371
Organic materials	−0·00213	−0·00462
Soil density	−0·00321	−0·00696
Soil specific heat	−0·00321	−0·00696
Initial soil water content	0·00557	0·01209
Lower layer soil water content	0·00818	0·01775
Initial soil temperature	0·00097	0·00212
Lower layer soil temperature	0·00299	0·00650
Air temperature	0·34519	0·74904
Air relative humidity	0·00017	0·00038
Wind speed	−0·05514	−0·11965
Global radiation	0·12829	0·27838
Soil layer thickness	−0·01062	−0·02303
Surface layer thickness	−0·00098	−0·00214
Saturated hydraulic conductivity	0·00625	0·01357

temperature, which account for 0·128%, 0·093% and 0·047% of the surface temperature. An increase of 1% in soil layer thickness would lead to about 0·01°C decrease of surface temperature, accounting for 0·023%. The model appears to be insensitive to the change of other parameters, including soil thermal conductivity, soil composition structure, initial soil temperature, soil water content and so on. As indicated in Table 1, a 1% change of these parameters would lead to less than 0·01°C or less than 0·02% change of surface temperature. Their insensitivity implies that the modeling result of LST change will not be obviously shaped by the possible small error of these parameters in preparation of the required data sets for the modeling.

Comparison of surface energy balance

Only a part of the global radiation reaching the ground surface is absorbed by the ground and hence enters the energy balance process of the land–air interface system. The remainder of the radiation is reflected back toward the atmosphere without affecting the surface temperature of the ground soil. The density of reflection or albedo largely determines the energy that drives the thermal movement of the ground soil. This can be clearly shown by the simulation results of the region. The comparison to the change of the main parts of surface energy balance is shown in Fig. 11. Due to much lower albedo of biogenic crust, the amount of net radiation on the crust surface is much greater than that on the bare sand during the day (Fig. 11(a)). The average net radiation on biogenic crust surface is as high as 585·69 $W m^{-2}$ in the hours 12:00–15:00, which is about 26·42% greater than that on the bare sand surface. This

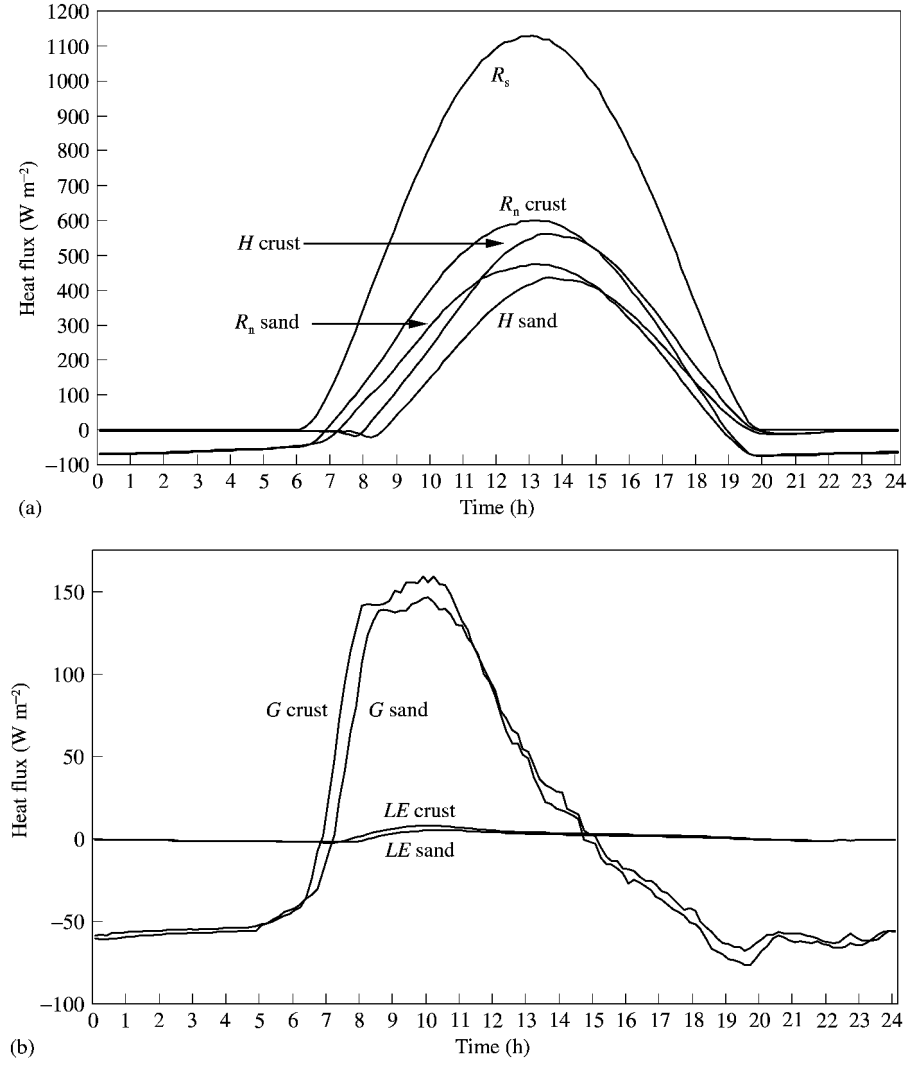

Figure 11. Comparison of simulated surface energy balance on biogenic crust and sand surfaces, illustrating (a) net radiation and sensible heat flux, and (b) soil heat and latent heat fluxes.

difference of net radiation is the main source of energy driving the thermal dynamics of the two surfaces.

The incident radiant energy that is not reflected by the ground surface is absorbed and converted into heat, which is then dissipated in several ways (Brutsaert, 1982). In an arid environment where little water is available for evaporation that consumes a lot of heat flux on the surface, sensible heat is the main mode of energy dissipation from the ground surface. In the sand dune region, sensible heat flux into the air accounts for above 90% of net radiation in the hours 12:00–15:00· However, the amount of heat on biogenic crust is much greater than that on bare sand. At about noon (12:30–14:30) when the surface temperature reaches its peak (Fig. 11(a)), the average sensible heat into the atmosphere is about 550·13W m^{-2} on biogenic crust and 423·24W m^{-2} on sand surface. The former is above 1/4 (29·98%) higher than the latter. Because the sensible

heat is proportional to the temperature difference between the surface and the air near the surface, the greater the heat the greater is the temperature difference under the same conditions of wind speed and surface roughness length. Given the same air temperature, this means that the biogenic crust surface is much hotter than the bare sand.

The change of soil heat and latent heat flux is shown in Fig. 11(b), from which we can see that the two heat fluxes are much less than sensible heat fluxes into the air. In the case of biogenic crust surface, the average soil heat is only about $63{\cdot}14\,\mathrm{W\,m^{-2}}$ at the noon 12:00–13:00, which only accounts for about 10·68% of the net radiation and 5·65% of the global radiation. And at this time, the average latent heat is only about $4{\cdot}36\,\mathrm{W\,m^{-2}}$, accounting for 0·74% of the net radiation. The soil heat flux on bare sand is a little bit greater than that on biogenic crust. At about noon, the average soil heat on bare sand is about $68{\cdot}12\,\mathrm{W\,m^{-2}}$ and latent heat $3{\cdot}36\,\mathrm{W\,m^{-2}}$, accounting for 14·67% and 0·72% of its net radiation. This implies that heat transfers more strongly to the soil on sand surface than on biogenic crust, while the evaporation, in spite of being very weak, is relatively stronger from biogenic crust than from sand surface at about noon. Compared with net radiation and sensible heat flux, the conclusion can be drawn that the amount of these two parts is too small to have a significant effect on the surface temperature change.

From the latent heat flux we can estimate the net loss of soil moisture per day in the hot summer season. The total amount of latent heat flux is $270{\cdot}15\,\mathrm{W\,m^{-2}}$ on the biogenic crust and $190{\cdot}33\,\mathrm{W\,m^{-2}}$ on the sand surface. Thus, the total evaporation is about $0{\cdot}066\,\mathrm{kg\,day^{-1}\,m^{-2}}$ from the biogenic crust and $0{\cdot}047\,\mathrm{kg\,day^{-1}\,m^{-2}}$ from bare sand. The negative latent heat flux during the night also indicates that there is a process of dew formation, which releases some energy for the balance of the system. The total negative latent heat flux is about $77{\cdot}95\,\mathrm{W\,m^{-2}}$ on biogenic crust and $90{\cdot}52\,\mathrm{W\,m^{-2}}$ on active sand, corresponding to 0·019 and 0·022 kg of dew formation, respectively. This simulation result of dew formation amount is very close to the measurement of Kidron (1999) in the region. The main reason for more dew forming on bare sand surface during the night probably is that it has a relatively lower LST than biogenic crust. Balanced from evaporation and dew absorption, the net soil moisture lost in the arid environment is about $0{\cdot}047\,\mathrm{kg\,day^{-1}m^{-2}}$ on biogenic crust and $0{\cdot}025\,\mathrm{kg\,day^{-1}\,m^{-2}}$ on active sand. The result also indicates that evaporation is slightly stronger from biogenic crust than from active sand. This explains the difference of soil moisture content observed in the hot summer season in the layers under the two typical surfaces.

The change of the above main parts of the surface energy balance experiences a different process in the night-time when there is no solar radiation. Figure 11(a) indicates that net radiation and sensible heat into the air are negative on both surfaces. And negative soil heat flux and latent heat flux can also be seen in Fig. 11(b). This implies that during the night the surface energy reaches balance by getting heat flux from both the air and the soil. However, the heat flux released from the soil and the air is quite small and it does not exceed $80\,\mathrm{W\,m^{-2}}$. Another feature is that the heat flux seems to be stable during the night. The dew forming on the two surfaces during the night quickly evaporates in the early morning when the sun comes up. Thus, the maximal latent heat appears at about 9:00–10:00 (Figure 11(b)) and it is about $7\,\mathrm{W\,m^{-2}}$ for biogenic crust and $5\,\mathrm{W\,m^{-2}}$ for active sand. This evaporation process explains the rapid ascendance of the surface temperature in the morning.

Change of main parameters in the surface energy balance

Analysis of the change of main parameters in the system can also assist in understanding the difference of surface energy balance on the two surface patterns.

As indicated above, sensible heat flux into the atmosphere is the main way of dissipating the energy absorbed by the ground. According to Eqn (3), sensible heat

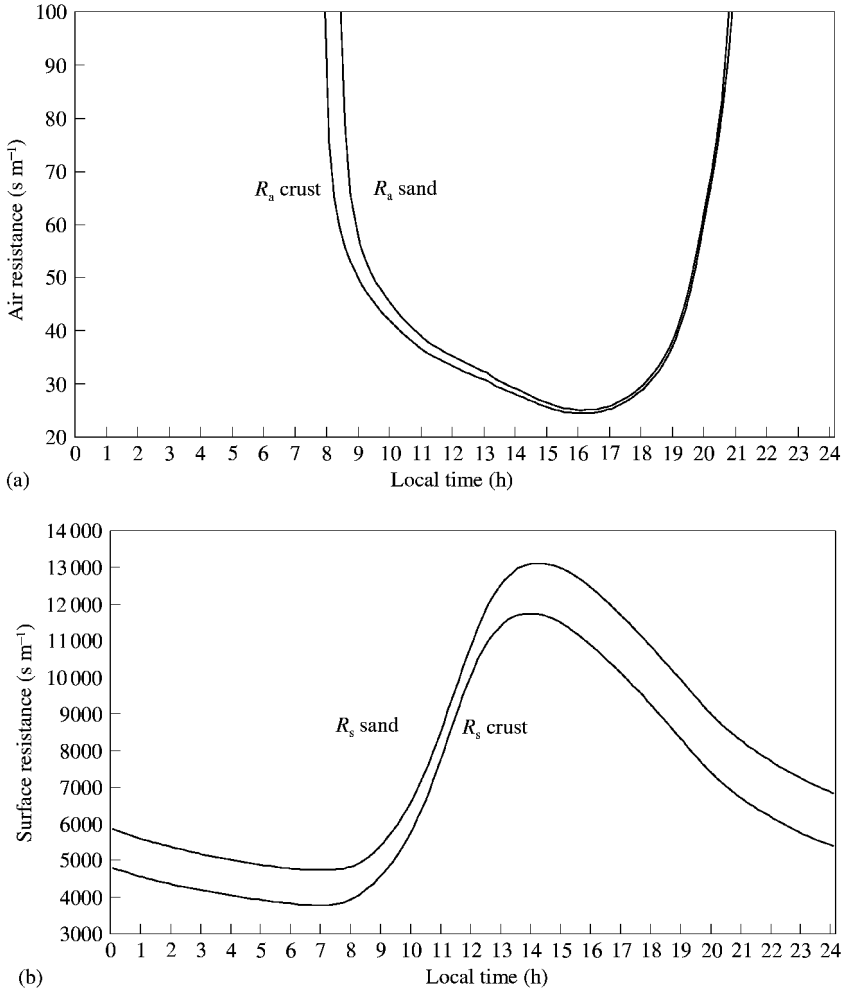

Figure 12. Comparison of (a) air heat resistance and (b) surface resistance to evaporation on biogenic crust and bare sand surfaces.

flux into the air is proportional to the land–air temperature difference and inversely proportional to air heat transfer resistance. Given that the air density and heat capacity show little variation in the temperature range, sensible heat into the air is mainly contributed by the land–air temperature difference. On the other hand, air heat resistance also plays an important role in governing sensible heat flux (Lhomme *et al.*, 1994). Figure 9.3(a) compares the air heat resistance of the two surface patterns. Generally speaking, the change of air heat resistance is similar for the two surface patterns, especially in the daytime. This is mainly because air heat resistance is determined by wind speed and we assume the same wind velocity for the two surfaces. Although the air heat resistances between the two surfaces are very close, a slight difference can still be seen (Fig. 12(a)), being greater on bare sand than on biogenic crust. During the day, land–air temperature difference is big and wind speed is high. Thus, heat is easily transferred into the air. From 8:30 to 19:30, air heat resistance of the two surfaces is rather small. Minimal air heat resistance occurs in the late afternoon at about 16:00–17:00 when the wind is the strongest. Maximal resistance

occurs at about midnight when wind speed declines to the lowest. During the night air resistance is much higher than during the day. Very big air heat resistance during the night makes the sensible heat flux quite small.

Surface resistance to evaporation is also a very important factor in determining the evaporation rate and hence the latent heat flux (Van Bavel *et al.*, 1976; Brutsaert, 1982; Garratt, 1984). In an arid environment, soil water content is extremely low, surface resistance to evaporation is very high. As indicated in Fig. 12(b), surface resistance to evaporation is generally greater on sand than on biogenic crust. This is because biogenic crust has a little bit higher surface soil moisture content than bare sand (Fig. 13(a)). Maximal resistance occurs in the early afternoon when surface water content is the lowest due to consecutive evaporation in the previous hours. Surface resistance to evaporation is as high as $13{,}000\,s\,m^{-1}$ on bare sand and $12{,}000\,s\,m^{-1}$ on biogenic crust in the early afternoon. Minimal surface resistance to evaporation can be seen at dawn when the surfaces have the highest moisture content due to their absorption of dew during the night. Actually, the change of surface resistance to evaporation is in accordance with the fluctuation of soil moisture content in the surface layer.

Availability of soil moisture is one of the three critical conditions for evaporation. The amount of water in the soil directly affects the amount of energy consumed to evaporate water (Williams & Balling, 1996). In the border region, the soil moisture is very low during the hot dry summer. The small evaporation in the border region (Fig. 11(b)) is mainly due to its extremely low level of soil water content. Figure 13(a) compares the change of volumetric water content of the two surface patterns. The surface moisture change shown in Fig. 13(a) is in accordance with our measurements of soil water change given in the previous section. The surface moisture of biogenic crust is obviously higher than that of bare sand, even though their absolute difference is only about $0{\cdot}6\,kg\,m^{-3}$ during the day. In the daytime, surface moisture tends to decline because of evaporation. The moisture content reaches minimum in the early afternoon at about 13:00–15:00 when LST is very high. In the night-time the surface absorbs some moisture from the air, which makes its moisture content gradually increase till dawn at about 6:00 (Fig. 13(a)).

Comparison of soil moisture content at 10 and 20 cm depth is also plotted in Fig. 13(a). Due to little heat flux penetrating into the lower layers of the profile, soil moisture content showed less fluctuation with the depth of 20 cm. At a depth of 10 cm, soil moisture shows very small daily change and at 20 cm the change is little. Another important feature is that soil moisture content at 10 cm depth is greater under biogenic crust surface than under bare sand surface. However, the situation at 20 cm is the opposite. Soil moisture content under biogenic crust is less than that under sand surface. This is in accordance with what we observed in the measurements of soil water content.

Under unsaturation, soil relative humidity is mainly dependent on soil water content though temperature is also an important determinant. Figure 13(b) shows the change of soil relative humidity on the two surfaces. The change is similar to that of the surface moisture content. During the night, biogenic crust has a little bit higher surface relative humidity than active sand. In the morning, the relative humidity of sand surface is higher than that of biogenic crust. However, in the afternoon, biogenic crust has a little bit higher relative humidity than bare sand. This may be because the soil under biogenic crust has higher hydraulic conductivity and the biogenic crust has a greater evaporation rate than bare sand (Fig. 11(b)).

Comparison of surface vapor pressure on the two surfaces is illustrated in Fig. 13(c), which also plots air vapor pressure as a reference. According to Eqn (6), evaporation from the surface occurs when vapor pressure of the surface is greater than the air and dew formation occurs when the air vapor pressure is greater than the surface. From Fig. 13(c) we can see that the vapor pressure of the two surfaces is

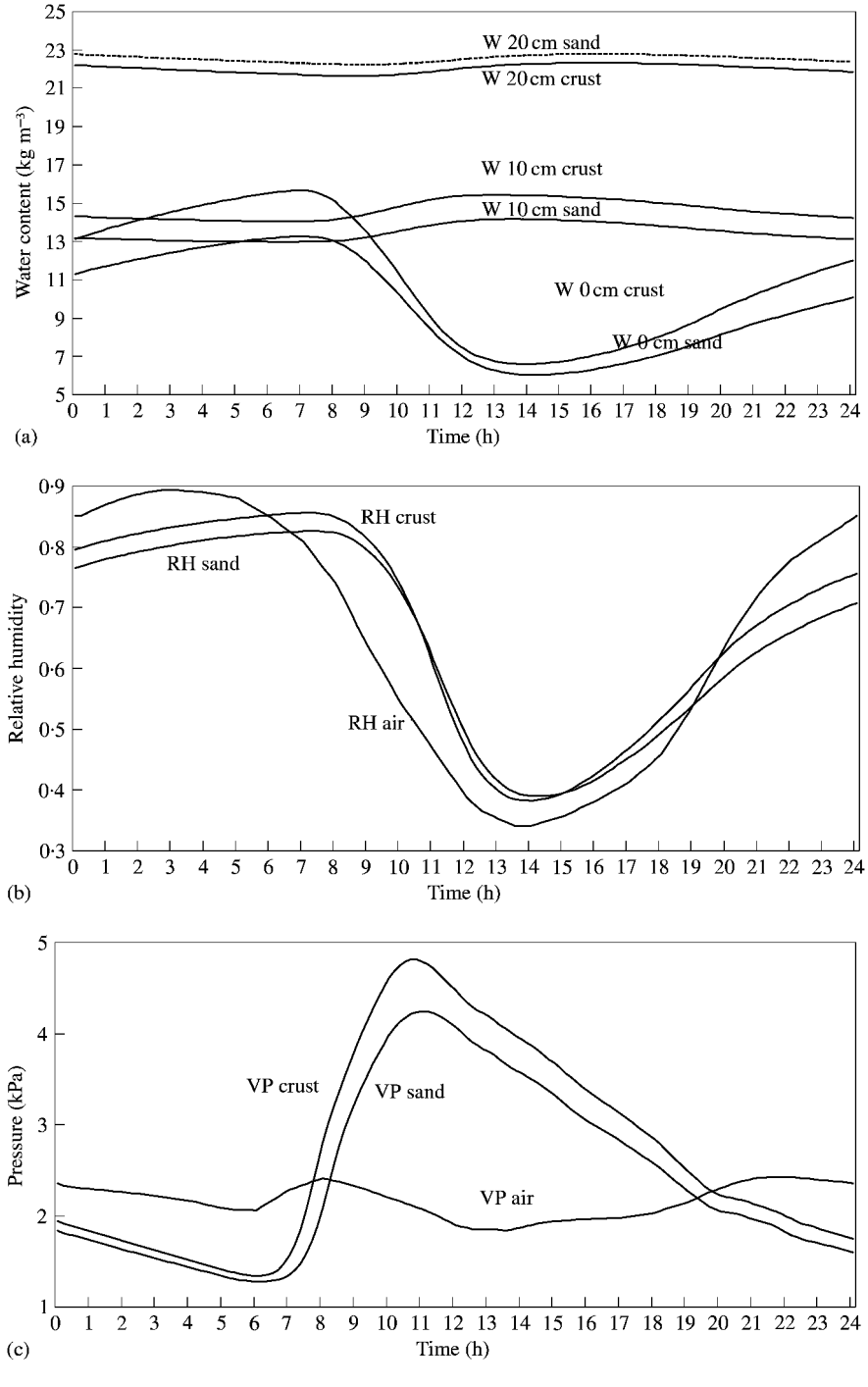

Figure 13. Comparison of (a) soil moisture content, (b) surface relative humidity and (c) surface vapor pressure on biogenic crust and sand surfaces.

greater than air vapor pressure in the daytime from about 8:00 to about 20:00. This means that evaporation from both surfaces occurs during this period even though it is rather weak. Dew formation also occurs in the arid environment during the night because air vapor pressure is greater than surface vapor pressure. However, a comparison of the area between surface vapor pressure and air vapor pressure reveals that evaporation is greater than vapor absorption, as described above. Figure 13(c) also indicates that biogenic crust has a higher surface vapor pressure than bare sand surface. This implies that evaporation from biogenic crust is relatively stronger than that from active sand. The lower vapor pressure of sand surface during the night also indicates more dew formation on bare sand surface than on biogenic crust, as mentioned above.

Contribution of leading factors to surface temperature difference

Based on the above modeling results, we try to isolate the contribution of the leading factors to the surface temperature difference on the two surfaces. Assuming the same effects in terms of such meteorological factors as global radiation, wind speed and air temperature, the leading factors of the model that may lead to the difference of surface temperature between the two surface patterns can be distinguished as albedo, surface emissivity and soil properties especially soil moisture.

The difference of surface albedo between biogenic crust and bare sand has an important effect on the LST difference of the two surface patterns. As we have seen in the previous section, biogenic crust has an albedo of about 13% lower than bare sand. Thus, under the same global radiation, biogenic crust absorbs much more energy from the incident radiation than bare sand. The simulation indicates that the difference of albedo accounts for more than 86% of net radiation difference between the two surfaces. As shown in Fig. 11(b), the average difference of surface temperature between the two patterns is 2·63°C in the hours 12:00–15:00. Using the albedo of biogenic crust and the sand soil properties for simulation, we obtain the average surface temperature of 49·25°C in the same period, which is about 2·31°C higher than LST of bare sand and 0·32°C lower than LST of biogenic crust. Therefore, we can conclude that about 87·83% of the surface temperature difference between the two surfaces is contributed by its albedo difference.

The simulation indicates that surface emissivity difference has little effect on the LST difference between the two surface patterns. We also test the contribution of surface emissivity difference to the LST difference of the two surface patterns. Using the emissivity of biogenic crust and soil properties of bare sand for simulation, we find that the surface emissivity difference can only lead to about 0·05°C of LST change from the LST of biogenic crust. This implies that the difference of surface emissivity can only explain about 1·90% of the LST difference between the two surfaces.

The difference of soil properties especially soil moisture also has an important effect on the LST difference between the two surface patterns. As mentioned above, soil properties are different under the two surfaces. The soil under biogenic crust has higher water content in the upper layers and lower soil moisture content in the lower layers. Consequently, evaporation from biogenic crust surface is greater than that from bare sand. Due to the different soil constituents, the surface layer of bare sand has much higher thermal conductivity than biogenic crust. Higher thermal conductivity of bare sand makes its heat transfer a little bit faster into the subsoil than it is in biogenic crust. Moreover, higher heat capacity in the subsoil of bare sand due to its higher soil moisture content also makes it more difficult to be heated than the subsoil under the biogenic crust. Soil heating process has proportional correlation to the change of surface temperature and evaporation. The combined functioning of these two aspects makes the soil temperature increase slightly easier under biogenic crust than under

bare sand. And this finally shapes the different change of their surface temperature regime and energy balance on the two surfaces.

It is really difficult to separate the effect of all soil properties on LST change because they are interrelated to each other. Therefore, we roughly count their effect as the remainder of the total minus the effect of albedo and ground emissivity. In this way, the difference of soil properties especially, soil moisture, accounts for about 10·27% of the total LST difference between the two surface patterns.

Given the strong solar radiation in the summer season, the thin surface layer (1–5 mm) of biogenic crust can be easily heated in spite of its relatively higher moisture content. In the arid environment, soil water content is extremely low and evaporation can only consume a very small part of the total energy absorbed by the surface. As indicated in Fig. 11(b), at 12:00–15:00 evaporation only accounts for about 0·61% of net radiation in the case of bare sand and for 0·65% in the case of biogenic crust. This small percentage of latent heat flux has little effect on the cooling down of the ground surface. As a result, the surfaces experience different warming processes due to the differences in absorbed incident sky radiation. Obviously, the surface energy absorption accumulates more in the upper biogenic crust layer than the bare sand surface layer. And this makes the surface of biogenic crust hotter than that of bare sand. Even though the involved process is rather complicated, the mechanism is very clear, i.e. the greater amount of main surface flux components on biogenic crust makes its surface temperature more difficult to reach its surface energy balance at a higher level than it is on bare sand surface.

Understanding thermal variation on both sides of the region

The above analysis and explanation of surface temperature difference on the two typical surface patterns can be extended to the understanding of surface temperature difference and thermal variation on both sides of the Israel–Egypt border region. The Israeli side has above 72% of biogenic crust cover and the Egyptian side above 80% of bare sand surface (Qin & Karnieli, 2000). Their surface albedo difference is also very obvious, as indicated in the previous section. The lower surface albedo on the Israeli side makes it absorb much more incident solar energy and atmospheric emittance. Although most of the net radiation returns into the atmosphere as sensible heat, the remainder is still obviously greater on the Israeli side than on the Egyptian side and this remainder is very strongly related to the surface and soil temperature change and soil moisture movement. During the hot summer season, the region is very dry. Most vegetation is in dormancy (Otterman & Tucker, 1985; Karnieli & Tsoar, 1995). Leaves of shrubs reduce to minimum and more than two-third of canopy is dead according to our field observation. The dead canopy is not only out of functioning evaporation but also forms the debris that absorbs more incident radiation due to its darker tone and hence lower albedo. Even though the Israeli side has more vegetation, the evaporation contributed by the vegetation is still very small in comparison with the net radiation. Together with the transpiration contribution of vegetation, the average evapo-transpiration at 12:00–15:00 on the Israeli side is estimated to be about $41 \mathrm{W\,m^{-2}}$, accounting for 7% of the net radiation. This small latent heat flux has little effect on the surface energy balance process in the arid environment. LST change in the arid environment is then mainly controlled by the amount of incident solar energy absorbed by the ground as soil heat. Therefore, the anomalous LST change and thermal variation on both sides of the region can still be explained as the direct result of the obvious albedo difference on both sides, as Otterman (1974) did. This albedo difference is mainly caused by the sharp contrast of surface composition on both sides. As mentioned above, the Israeli side has much more biogenic crust while the Egyptian side is mainly dominated by bare soil and active sand as a result of overgrazing.

Considering this sharp contrast, the LST anomaly observed on remote sensing images can be understood as the result of spectral functioning difference of biogenic crust and bare sand on both sides of the region.

Soil properties on the Israeli side can be viewed as similar to those of biogenic crust and on the Egyptian side similar to those of bare sand. This similarity can be used to understand soil heat transfer on both sides of the region. As mentioned above, the heat accumulating on the surface of biogenic crust is greater than that on bare sand, due to the difference of soil properties especially soil thermal conductivity. This functioning process also exists on both sides of the region because of their surface composition difference. Most of the surface on the Israeli side is covered with biogenic crust which has lower thermal conductivity while the surface of the Egyptian side is dominated by bare sand having relatively higher thermal conductivity. Therefore, we can expect that the Israeli side has more heat accumulation on its surface due to its relatively lower thermal conductivity than the Egyptian side. Finally, the ground on the Israeli side has higher surface temperature. Therefore, except for the main contribution of spectral functioning difference of biogenic crust and active sand, subsoil properties as a whole are the second main factor leading to the anomalous LST change and thermal variation observed in the border region.

Comparison with Charney's classic studies and other related studies

In the mid-1970s, Charney and his co-workers conducted a series of studies on the interaction between desertification and climate in Sahel and other dryland regions (Charney, 1975; Charney *et al.*, 1975, 1977). They proposed a biogeophysical feedback model, also dubbed albedo model (Williams & Balling, 1996). On the basis of their investigation of Sahel and Sahara drought, Charney and his co-workers argued that overgrazing due to settlement and over-population in arid and semi-arid regions will lead to the reduction of vegetation cover and hence to an increase in surface albedo. Consequently, the increased albedo will decrease surface net radiation, result in surface cooling and lower ground surface temperature, promote subsidence of air aloft, reduce convection and cloud formation, thereby reducing regional rainfall in the arid and semi-arid regions. Additional drying in the Sahel region leads to regional climatic desertification which positively feeds back to the overgrazing and follows the circling procedures. Using a general circulation model developed for meso-scale regional atmospheric and climate simulation, they demonstrated the important effect of albedo on regional climate, especially rainfall in Sahel, Sahara and other dryland regions. The propositions and assumptions underpinning the studies became known as Charney hypothesis (Williams & Balling, 1996). Based on the simulation with two different surface albedos (low albedo 14% represents low human stress and high albedo 35% the high stress due to overgrazing), Charney *et al.* (1975) found that the mean rainfall over Sahara during the calendar month of July decrease by about 43% from low-albedo to high-albedo experiments. And the results from the high-albedo experiment are quite close to the observed distribution of rain in Sahara summer. Thus, they concluded that surface albedo can have a sustantial effect on climate in Sahara and very local changes in albedo may be sufficient to produce droughts.

It seems that the higher surface albedo leading to higher surface temperature in the border region of our study supports the Charney hypothesis about the function of albedo in climate change. Close comparison still finds some differences between our study and that of Charney. In Charney's studies, it is assumed that overgrazing leads to the reduction of vegetation cover, which in turn leads to the increase in surface albedo. Thus, the importance of albedo in Charney's biogeophysical feedback model is based on the direct relationship between vegetation and surface albedo. In the border region, the obvious difference of surface albedo across the border is not only

due to the vegetation difference, but also due to the biogenic crust difference (Karnieli & Tsoar, 1995). Overgrazing on the Egyptian side not only causes the reduction of vegetation, but also prevents the establishment of biogenic crust on the surface. Actually, it is the biogenic crust difference that leads to the substantial difference in albedo across the border. Desert plants, which still have much higher evapo-transpiration, contribute much less to the albedo difference across the border. Despite the support from a variety of modeling studies, the Charney hypothesis was vigorously challenged on theoretical and empirical grounds (Williams & Balling, 1996). Since Charney's model is based on the direct contribution of vegetation to albedo, its assumption about the higher surface albedo leading to higher surface temperature has not been seen in other arid regions. This is mainly because the lower albedo contributed by more vegetation cover still has higher evapo-transpiration that prevents the increase of surface temperature. On the other hand, since the bare surface as a result of vegetation removal is easy to be dried and hence has very low top-soil moisture that prevents soil heat transfer into lower layers, the surface with high albedo contributed by low vegetation still has relatively higher surface temperature. This has been observed across the US–Mexico boder (Balling, 1989). Only in the region where lower surface albedo is not prevalently contributed by vegetation and where soil moisture is very low such as our region, the phenomenon of higher surface albedo leading to lower surface temperature is possible.

Another important condition for the occurrence of surface temperature anomaly across the border is the very low soil moisture in the region. Many numerical modeling studies showed that soil moisture is also very important in affecting climate change in the arid and semi-arid regions (Williams & Balling, 1996). Cunning & Rowntree (1986) demonstrated that Sahara climate is related not only to surface albedo change but also to soil moisture changes and the importance of soil moisture could override the changes to the albedo. Combining the local energy balance model with a global climate model, Lanicci *et al.* (1987) found that soil moisture changes in the drylands of the American Great Plains could have an important impact on the location and intensity of convective storms. Franchito & Rao (1992) developed a global model that includes detailed biogeophysical feedbacks to simulate the effects of desertification and found that desertification causes a reduction in local net radiation, soil moisture, evaporation and precipitation which consequently results in an increase in local surface and near-surface temperature. In our region, the soil moisture is extremely low during the hot dry summer. Our field sampling found an insignificant difference in soil moisture of the top layer under bare sand and biogenic crust. The insignificant difference in soil moisture between the two main surface patterns which, respectively, represents the surface on both sides makes it easy to understand its relatively less importance than albedo in leading to the occurrence of the surface temperature anomaly across the border.

Conclusion

An anomalous thermal phenomenon was observed in the daytime remote sensing images in the sand dunes across the Israel–Egypt border. This interesting phenomenon has not been thoroughly studied for understanding its occurrence, especially from the viewpoint of micrometeorological modeling. A complete surface energy balance model that couples soil temperature change simultaneously with soil moisture dynamics has been established in the paper in order to simulate the surface temperature change and heat flux variation of the region. Various measurements have been conducted at the Nizzana Research site on the Israeli side of the region for the required simulation data. Using the data and the numerical solution methodology of

the model, the surface temperature and heat flux change has been simulated on the two most important surface patterns of the region: biogenic crust representing the Israeli side and bare sand representing the Egyptian side.

Simulation results indicate that the surface temperature of biogenic crust and bare sand in summer can reach as high as about 48–50°C. According to the model, biogenic crust does have a surface temperature of about 2·5–2·8°C higher than bare sand in the hours 12:00–15:00. During the night, the difference of surface temperature between biogenic crust and bare sand is not obvious. A sensitive analysis of the model indicates that the largest change in T_s is observed in a small change of air temperature and global radiation, which is followed by surface albedo, roughness length and surface emissivity. A 1% increase of air temperature and global radiation will lead to 0·75% and 0·28% increase of LST. And the same amount of surface albedo, roughness length and emissivity increase will result in 0·13%, 0·09% and 0·05% decrease of surface temperature. Comparison of surface energy balance reveals that the average net radiation of biogenic crust can reach up to $585{\cdot}69\,\mathrm{W\,m^{-2}}$ in the hours 12:00–15:00, which is about 26·42% higher than that of active sand. More than 85% of net radiation returns into the air as sensible heat flux. The average soil heat flux of biogenic crust is about $63{\cdot}14\,\mathrm{W\,m^{-2}}$ in the noon hour 12:00–13:00, accounting for 10·68% of net radiation. The amount of soil heat flux is a little bit greater on sand surface than on biogenic crust. Due to little soil moisture available for evaporation, latent heat flux of biogenic crust is only $4{\cdot}14\,\mathrm{W\,m^{-2}}$ at noon, accounting for 0·74% of net radiation. For the bare sand, latent heat is only $3{\cdot}36\,\mathrm{W\,m^{-2}}$ and accounts for 0·72% of its net radiation. Daily evaporation of the region is very small under the arid environment. Net soil water loss due to evaporation is estimated to be about $0{\cdot}047\,\mathrm{kg\,day^{-1}}$ on biogenic crust and about $0{\cdot}025\,\mathrm{kg\,day^{-1}}$ on bare sand. Negative latent heat flux during the night also indicates the formation of some dews on both surfaces. But bare sand surface, due to its relatively lower LST at night, seems to obtain more moisture from the air than biogenic crust. This difference in surface energy balance also produces different change of subsoil properties especially soil moisture content at various depths and the surface vapor pressure and relative humidity. The mutual connection of these changes finally determines LST difference and thermal variation on the two typical surface patterns of the region.

The LST anomaly on both sides of the border region can be understood in several ways. First of all, surface composition difference between the two sides is the direct reason for the LST anomaly. The Israeli side is mainly composed of biogenic crust, which covers about 72% of the surface. Bare sand only accounts for about 7% of its surface. However, the Egyptian side is mainly covered with bare sand, which accounts for above 80% of the total area. Biogenic crust and vegetation only account for about 12% and 4·5% of the total surface area. With the assumption of similar atmosphere and similar subsoil composition and formation on both sides, this difference of surface composition directly explains the occurrence of the LST anomaly on both sides even though the functioning mechanics of the process is rather complicated.

Second, the surface composition difference on both sides leads to the difference of surface and subsoil properties. The combined functioning of this surface and subsoil property difference makes the LST change on both sides appear to be of difference in its expression. The coherent mechanics can be understood through the simulation results of surface energy balance model. According to their surface composition, the Israeli side can be represented with biogenic crust and the Egyptian side with bare sand. Simulation results indicate that biogenic crust and bare sand do have an obvious LST difference under the assumption of the same global radiation, wind speed, air temperature and relative humidity. The LST difference between the two surface patterns can reach up to about 2·5–2·8°C in the early afternoon when satellite passed and observed the LST of the region. The most important factor leading to the LST difference of the two surface patterns is surface albedo, which accounts for

about 87·83% of the LST difference between the two surfaces. Subsoil properties also have a significant effect on the LST difference of the two surface patterns. It can explain about 10·27% of the LST difference. Although surface emissivity has significant difference on the two typical surface patterns and hence on both sides, it can only account for about 1·90% of the LST difference between the two surfaces.

Third, the mechanism of the LST difference on the two typical surface patterns can be summarized as follows. The biogenic crust surface has much lower surface albedo. Thus, it absorbs much more incident sky radiation than bare sand surface. Even though most of the absorbed energy is dissipated as sensible heat into the air, the remainder of the absorbed energy is also much more on the biogenic crust than on the bare sand. This remainder energy is dissipated mainly in two ways: heat into the soil and evaporation. Because soil water content is extremely low in the arid environment, evaporation only accounts for about 0·5–1% of the total net radiation. Therefore, the slightly higher evaporation on biogenic crust is not enough to cool down the much higher surface temperature due to greater absorption of the incident radiation in the arid environment.

The difference of soil composition in the surface layer plays an important role in shaping LST change on the two surfaces. Due to higher quartz content, thermal conductivity of surface layer on bare sand is greater than that on biogenic crust even though the latter has a little bit more soil moisture content. At a depth of about 10–15 cm onward, the subsoil under bare sand has more moisture content than the subsoil under biogenic crust. Consequently, this changes the soil properties under the two typical surfaces. Higher soil thermal conductivity of surface layer on bare sand makes its soil heat transfer a little bit easier than it is on biogenic crust. In other words, heat is more difficult to go down into the lower layers under biogenic crust and easier to accumulate in the upper thin layer of biogenic crust. This makes its surface temperature even easier to ascend.

Finally, this mechanism of heating process difference on the two typical surface patterns can be extended to understand the LST anomaly on both sides of the region. During the hot summer season, the region is very dry and vegetation is in dormancy. Leaves of most shrubs reduce to minimum. Even though the Israeli side has more vegetation, the evapo-transpiration contributed by the vegetation is still very small in comparison with the net radiation. This small latent heat flux has little effect on the surface energy balance process in the arid environment. LST change in the desert region is mainly controlled by the amount of incident solar energy absorbed by the ground as soil heat. Therefore, the anomalous LST change and thermal variation on both sides of the region can still be explained as the direct result of the obvious albedo difference on both sides. This albedo difference is mainly caused by the sharp contrast of surface composition on both sides as a result of spectral functioning difference between biogenic crust and bare sand. On the other hand, the Israeli side has a stronger evaporation rate than the Egyptian side. This means that the soil water content may be easier to lose on the Israeli side than on the Egyptian side where bare sand prevails. After a long time of consecutive evaporation in the hot summer, the subsoil of Israeli side on average may have less soil moisture than that of the Egyptian side. And this property together with the low thermal conductivity of the crust may finally exacerbate soil heat accumulation on its surface layer (the thin biogenic crust). As a result, this makes its surface temperature easily increased. On the Egyptian side, relatively higher subsoil moisture content combined with the relatively greater thermal conductivity of the sand will speed up its soil heat transfer from the surface into the lower layers. This can also intensify the existing LST anomaly on both sides.

The authors would like to thank Dr Heike Schmid, their colleague at the Remote Sensing Laboratory, for helping to access the study region for various measurements,

Dr Simon Berkowics, the administrator of The Arid Ecosystems Research Center, Inst. of Earth Sciences, The Hebrew University of Jerusalem, for offering the permission to conduct the required measurements in the Nizzana Research site and providing the rainfall data about the region, and Dr Thomas Litmann, Institute of Geography, Martin Luther University, Germany for providing one-month data of his measurements on air temperature, air relative humidity and wind speed of the region.

References

Balling Jr, R.C. (1989). The impact of summer rainfall on the temperature gradient along the United States–Mexico border. *Journal of Applied Climatology*, **28**: 304–308.

Berliner, P. (1988). Contribution of heat dissapated at the soil surface to the energy balance of a citrus orchard. Ph.D. thesis, Hebrew University, Jerusalem, Israel.

Blad, B.L. (1983). Energy exchange among leaf, canopy and environment. In: Teare, I.D. & Peat, M.M. (Eds), *Crop-Water Relations*, pp. 1–39, New York, U.S.A.: John Wiley and Sons, 547pp.

Bristow, K.L., Campbell, G.S., Papendick, R.I. & Elliott, L.F. (1986). Simulation of heat and moisture transfer through a surface residue-soil system. *Agricultural and Forest Meteorology*, **36**: 193–214.

Brutsaert, W. (1982). *Evaporation into the Atmosphere: Theory, History and Application*. Dordrecht, The Netherlands: D. Reidel Publishing Company, 299 pp.

Charney, J.G. (1975). Dynamics of deserts and drought in the Sahel. *Quarterly Journal of the Royal Meteorological Society*, **101**: 193–202.

Charney, J.G., Stone, P.H. & Quirk, W.J. (1975). Drought in the Sahara: a biogeophysical feedback mechanism. *Science*, **187**: 434–435.

Charney, J.G., Quirk, W.J., Chow, S. & Kornfield, J. (1977). A comparative study of the effects of albedo change on drought in semi-arid regions. *Journal of Atmospheric Sciences*, **34**: 1366–1385.

Chen, D.X. & Coughenour, M.B. (1994). GEMTM: a general model for energy and mass transfer of land surfaces and its application at the FIFE sites. *Agricultural and Forestry Meteorology*, **68**: 145–171.

Choudhury, G.J., Reginato, R.J. & S.B. (1986). An analysis of infrared temperature observations over wheat and calculation of latent heat flux. *Agricultural and Forest Meteorology*, **37**: 75–88.

Courault, D., Lagouarde, J.P. & Aloui, B. (1996). Evaporation for maritime catchment combining a meteorological model with vegetation information and airborne surface temperatures. *Agricultural and Forestry Meteorology*, **82**: 93–117.

Crank, J. & Nicolson, P. (1947). A practical method for numerical evaluation of solutions of partial differential equations of the heat conduction types. *Proceeding of Cambridge Philosophy Society*, **43**: 50–67.

Cunning, W.M. & Rowntree, P.R. (1986). Simulations of the Saharan atmosphere—dependence on moisture and albedo. *Quarterly Journal of the Royal Meteorological Society*, **112**: 971–999.

Diak, G. R. & Whipple, M.S. (1993). Improvements to models and methods for evaluating the land surface energy balance and 'effective' roughness using radiasonde reports and satellite-measured 'skin' temperature data. *Agricultural and Forest Meteorology*, **63**: 189–218.

Dolman, A.J. (1993). A multiple-source land surface energy balance model for use in general circulation models. *Agricultural and Forest Meteorology*, **65**: 21–45.

Dolman, A.J. & Blyth, E.M. (1997). Patch scale aggregation of heterogeneous land surface cover for mesoscale meteorological models. *Journal of Hydrology*, **190**: 252–268.

Franchito, S.H. & Rao, V.B. (1992). Climate change due to land surface alterations. *Climatic Change*, **22**: 1–34.

Friedl, M.A. (1996). Relationships among remotely sensed data, surface energy balance, and area-averaged fluxes over partially vegetated land surfaces. *Journal of Applied Meteorology*, **35**: 2091–2103.

Friedl, M.A. (1995). Modeling land surface fluxes using a sparse canopy model and radiometric surface temperature measurements. *Journal of Geophysical Research*, **100**: 25,435–25,446.

Gardner, C.M.K., Bell, J.D., Cooper, J.D., Dean, T.J. & Hodnett, M.G. (1991). Soil water content. In: Smith, K.A. & Mullins, C.E. (Eds), *Soil Analysis*, pp. 1–74. New York, USA.: Marcel Dekker Inc., 620 pp.

Garratt, J.R. (1984). The measurement of evaporation by meteorological methods. *Agricultural Water Management*, **8**: 99–117.

Gerson, R., Amit, R. & Grossman, S. (1985). *Dust Availability in Desert Terrain: a Study in the Deserts of Israel and the Sinai*. Israel: The Hebrew University of Jerusalem.

Ghildyal, B.P. & Tripathi, P. (1987). *Soil Physics*. New York, U.S.A.: John Wiley & Sons Ltd. 656 pp.

Hares, M.A. & Novak, M.D. (1992). Simulation of surface energy balance and soil temperature under strip tillage: I Model description. *Soil Science Society of America Journal*, **56**: 22–29.

Karnieli, A. (1997). Development and implementation of spectral crust index over dune sands. *International Journal of Remote Sensing*, **18**: 1207–1220.

Karnieli, A. & Sarafis, V. (1996). Reflectance spectrophotometry of cyanobacteria within soil crusts—a diagnostic tool. *International Journal of Remote Sensing*, **17**: 1609–1615.

Karnieli, A., Shachack, M., Tsoar, H., Zaady, E., Kaufman, Y. & Porter, W. (1996). The effect of microphytes on the spectral reflectance of vegetation in semi-arid regions. *Remote Sensing of Environment*, **57**: 88–96.

Karnieli, A. & Tsoar, H. (1995). Spectral reflectance of biogenic crust developed on desert dune sand along the Israel–Egypt border. *International Journal of Remote Sensing*, **16**:369–374.

Kidron, G.J. (1999). Altitude dependent dew and fog in the Negev Desert, Israel. *Agricultural and Forest Meteorology*, **96**: 1–8.

Kidron, G.J. & Yair, A. (1997). Rainfall–runoff relationship over encrusted dune surfaces, Nizzana, Western Negev, Israel. *Earth Surface Processes and Landforms*, **22**: 1169–1184.

Kimball, B.A. & Jackson, R.D. (1979). Soil heat flux. In: Barfield, B.J. & Gerber, J.F. (Eds), *Modification of the Aerial Environment of Plants*, pp. 211–229. St. Joseph, MI, U.S.A.: American Society of Agricultural Engineers. 538 pp.

Kutilek, M. & Nielson, D.R. (1994). *Soil Hydrology*. Destedt, Germany: Catena Verlag Ltd. 370 pp.

Lanicci, J.M., Carlson, T.N. & Warner, T.T. (1987). Sensitivity of the Great Plains severe-storm environment to soil moisture distribution. *Monthly Weather Review*, **115**: 2660–2673.

Lhomme, J.P., Monteny, B. & Amadou, M. (1994). Estimating sensible heat flux from radiometric temperature over sparse millet. *Agricultural and Forestry Meteorology*, **68**: 77–91.

Marshall, T.J. & Holmes, J.W. (1979). *Soil Physics*. Cambridge, UK.: Cambridge University Press. 345 pp.

McInnes, K.J. (1981). Thermal conductivity of soils from dryland wheat regions of Eastern Washington. M.S. thesis, Washington State University, Pullman, U.S.A.

Monteith, J.L. (1973). *Principles of Environmental Physics*. London, UK.: Edward Arnold Ltd. 241 pp.

Otterman, J. (1974). Baring high-albedo soils by overgrazing: a hypothesized desertification mechanism. *Science*, **186**: 531–533.

Otterman, J. (1977). Anthropogenic impact on the surface at the Earth. *Climatic Change*, **1**: 137–155.

Otterman, J. (1981). Satellite and field studies of man's impact on the surface in arid regions. *Tellus*, **33**, 68–77.

Otterman, J. & Fraser, R.S. (1976). Earth–atmosphere system and surface reflectivity in arid regions from Landsat multi-spectral scanner measurements. *Remote Sensing of Environment*, **5**: 247–266.

Otterman, J. & Robinove, C.J. (1982). Landsat monitoring of desert vegetation growth in 1972–1979 using a plant shadowing model. *Advance of Space Researches*, **2**: 45–50.

Otterman, J. & Tucker, C.J. (1985). Satellite measurements of surface albedo in semi desert. *Journal of Climate and Applied Meteorology*, **24**: 228–235.

Qin, Z. (1998). Surface composition structures on both sides of Israel–Egypt border region. Paper presented in *The 1st Academic Symposium of Chinese Students and Scholars in Israel*. Chinese Students and Scholars Association in Israel, Weizmann Institute of Science, Rehovot, Israel, December 17, 1998.

Qin, Z., Berliner, P. & Karnieli, A. (2002). Numerical solution of a complete surface energy balance model for simulation of heat fluxes and surface temperature under bare soil environment. *Applied Mathematics and Computation* **130**: 171–200.

Qin, Z., Karnieli, A. & Berliner, P. (2000). Remote sensing analysis of the land surface temperature anomaly in the sand dune region across the Israel–Egypt border. *International Journal of Remote Sensing* (accepted).

Qin, Z. & Karnieli, A. (2000). Quantitative estimation of land cover structure in the desert sand dunes across Israel–Egypt border using remote sensing data. *Remote Sensing of Envionment* (submitted).
Rose, C.W. (1979). *Agricultural Physics*. Oxford, UK.: Pergamon Press Ltd. 230pp.
Szeicz, G., Endrodi, G. & Tachman, S. (1969). Aerodynamic and surface factors in evaporation. *Water Resources Research*, **5**: 380–394.
Schmugge, T. & Humes, K. (1995). ASTER observations for the monitoring of land surface fluxes. *Journal of Japanese Remote Sensing Society*, **15**: 83–89.
Smith, G.D. (1978). *Numerical Solution of Partial Differential Equations: Finite Difference Methods*. Oxford, UK.: Oxford University Press. 304 pp.
Tsoar, H. & Karnieli, A. (1996). What determines the spectral reflectance of the Negev–Sinai sand dunes. *International Journal of Remote Sensing*, **17**: 3513–3525.
Tsoar, H. & Møller, J.T. (1986). The role of vegetation in the formation of linear sand dunes. In Nickling, W.P. (Ed.), *Aeolian Geomorphology*, Proceedings of the 17th Annual Binghamton Geomorphology symposium, September 1986, pp. 75–95. Boston, U.S.A.: Allen & Unwin Inc. 311 pp.
Van Bavel, C.H.M. & Hillel, D.I. (1976). Calculating potential and actual evaporation from a bare soil surface by simulation of concurrent flow of water and heat. *Agricultural and Forest Meteorology*, **17**: 453–476.
Verma, S.B. & Barfield, B.J. (1979). Aerial and crop resistance affecting energy transport. In: Barfield, B.J. & Gerber, J.F. (Eds), *Modification of the Aerial Environment of Plants*, pp. 230–248. St. Joseph, MI, U.S.A.: American Society of Agricultural Engineers. 538 pp.
Warren, A. & Harrison, C.M. (1984). People and the ecosystem: biogeography as a study of ecology and culture. *Geoforum*, **15**: 365–381.
Williams, M. A. J. & Balling, Jr, R.C. (1996). *Interactions of Desertification and Climate*. Prepared for World Meteorological Organisation, United Nations Environment Programme. London, U.K.: Arnold, 270 pp.
Yair, A., Lavee, H. & Greitser, N. (1997). Spatial and temporal variability of water percolation and movement in a sytem of longitudinal dunes, western Negev, Israel. *Hydrological Processes*, **11**: 43–58.
Yakirevich, A., Berliner, P. & Sorek, S. (1997). A model for numerical simulating of evaporation from bare saline soil. *Water Resources Research*, **33**: 1021–1033.
Zemel, Z. & Lomas, J. (1997). *Soil Temperature Regime in Israel as a Basis for Agricultural Planning and Activity*. Bet Dagon, Israel: Israel Meteorogical Service.

Appendix: Nomenclature

a_i, b_i, c_i	Coefficients in Eqn (28)
A_i, B_i, C_i	Coefficients in Eqn (29)
AVHRR	Advanced Very High Resolution Radiometer
c_a, c_m	Specific heat of air and clay, $J\,kg^{-1}\,K^{-1}$
c_q, c_w	Specific heat of quartz and water, $J\,kg^{-1}\,K^{-1}$
c_s	Specific heat of soil, $J\,kg^{-1}\,K^{-1}$
C_h	Change of soil water *vs.* relative humidity, $kg\,m^{-3}$
C_s	Volumetric soil heat capacity, $J\,m^{-3}\,K^{-1}$
d_i, e_i, f_i	Coefficient in Eqn (28)
D_i, E_i, F_i	Coefficient in Eqn (29)
dT	Small change in temperature, K
D_v	Apparent vapor diffusivity, $kg\,m^{-1}\,s^{-1}\,kPa^{-1}$
e	Soil vapor pressure, kPa
e_a, e_s	Air and surface vapor pressures, kPa
e_v	Saturated soil vapor pressure, kPa
g	Acceleration due to gravity, $g = 9{\cdot}8\,m\,s^{-2}$
g_j	Parameter in Eqn (24)
G	Soil heat flux, $W\,m^{-2}$
G_j	Parameter in Eqn (26)
h	Soil relative humidity
h_i	Soil relative humidity at the layer i
H	Sensible heat flux, $W\,m^{-2}$

i, j	The ith and jth soil layers
k	Von Karman constant, $k = 0{\cdot}4$
K_a, K_b	Parameters in Eqns (17) and (21)
K_c	Soil hydraulic conductivity, $kg\,s\,m^{-3}$
K_s	*S*oil thermal conductivity, $W\,m^{-1}\,K^{-1}$
L	Latent heat vaporization, $L = 2{\cdot}543 \times 10^6\,J\,kg^{-1}$
LE	Latent heat flux, $W\,m^{-2}$
LE_c	Energy driving soil water change, $W\,m^{-2}$
LST	Land surface temperature
n	Number of soil layers
NOAA	The National Oceanic and Atmospheric Administration
P_a	Atmospheric pressure, kPa
r_a	Air resistance coefficient to heat transfer, $s\,m^{-1}$
r_s	Surface resistance, $s\,m^{-1}$
R	Universal gas constant, R=461·52 $J\,kg^{-1}\,K^{-1}$
R_n	Net radiation, $W\,m^{-2}$
R_s	Global hemispheric radiation, $W\,m^{-2}$
s	Slope of saturated vapor pressure *vs.* temperature, $kPa\,K^{-1}$
T	Temperature, K
T_i,	Soil temperature at layer i, K
T_a, T_s	Air and surface temperatures, K
TM	Thematic Mapper
u_z	Wind velocity, $m\,s^{-1}$
V_a, V_m	Volumetric fraction of air and clay in soil
V_q, V_w	Volumetric fraction of quartz and water in soil
z	Standard height, $z = 2\,m$
z_0	Roughness length, m
Z_t	Parameter in Eqns (24) and (26)
ε_a, ε_s	Air and surface emissivities
φ_h, φ_m	Stability correction parameters for heat and momentum
ρ	Surface albedo
ρ_a, ρ_m	Density of air and clay, $kg\,m^{-3}$
ρ_q, ρ_w	Density of quartz and water, $kg\,m^{-3}$
ρ_s	Soil density, $kg\,m^{-3}$
σ	Stefan–Boltzmann constant, $\sigma = 5{\cdot}67 \times 10^{-8}\,W\,m^{-2}\,K^{-4}$
ψ	Soil water potential, $J\,kg^{-1}$
$\partial h/\partial t$	Rate of soil relative humidity change, s^{-1}
∂t	Time interval, s
$\partial T/\partial t$	Rate of soil temperature change, $K\,s^{-1}$
∂z	Depth of soil layer, m
$\partial\theta/\partial t$	Rate of soil water change, $kg\,m^{-3}\,s^{-1}$